technische universität
dortmund

Dissertation

Aspects of Stimulated Two-Photon Transitions in Bulk Semiconductors

submitted in partial fulfillment of the
requirements for the degree of

Dr. rer. nat.

to the Faculty of Physics at the
TU Dortmund University, Germany

by

Stephan Melzer

Dortmund, November 2019

Contents

Part I

Introduction

1 Motivation and Outline

Ever since the observation of saturable light absorption in organic dyes by *G. Lewis* in 1941 [LLM41], nonlinear optical phenomena have become a rich field of study and technological innovation in physics. Such a nonlinearity is generally referred to when the input property of a physical process itself alters the behaviour of the given interaction. For light-matter interactions being at focus in this work, the observation of nonlinear processes generally requires the irradiation of an intense light field upon a dielectric medium. Consequently, it was the advent of the laser as a source for strongly enhanced light fields which launched the research field of nonlinear optics after its invention by *T.H. Maiman* in 1960 [Mai60], when shortly after, the experimental discovery of second-harmonic generation in crystalline quartz by using a ruby optical maser reported by *P.A. Franken* in 1961 [Fra61] posed as the first discovery of a nonlinear optical process in solid state physics.

This thesis is centered around a nonlinear interaction involving two quanta of the electromagnetic field, referred to as photons, driving an electronic transition between two quantum levels in a solid state medium. More specifically, we intend to externally modify the two-photon absorption and stimulated emission property of a bulk semiconductor crystal. Formally, these two-photon processes act as a natural extension to the concepts of one-photon light-matter interactions which are present in every day life, manifested, for example, as absorption, reflection or diffraction of light, but obey a more complex set of mechanisms. Within this thesis, Chapter 2 discusses the relevant theoretical principles from both classical electrodynamics and quantum mechanics.

Historically, experiments on two-photon emission in particular have been conducted using atomic systems, where by addressing optical transitions between well defined electronic states in light element gases, both spontaneous [LNT65] and enhanced, or stimulated [YRB68] two-photon emission already has been demonstrated in the late 1960s. Some years later, the realization of two-photon lasing in atomic lithium [NZT81] and from barium dressed states [Gau92] has been reported. A transfer of stimulated two-photon emission to the semiconductor medium, as investigated in this work, is very attractive because of its inherently large and fast optical nonlinearities [ACP89] and the capability to inject such materials with very high carrier densities, making it possible to macroscopically utilize this comparatively weak higher order

processes. This results in promising technological applications, not least due to the scalability of semiconductor systems. First of, the stimulated "duplication of photons" in this process being bound to energy and polarization conservation laws serves as a source of entangled photons [HGO07], which are essential for practical quantum information processing [Cla69; Wal03; Kum04]. Secondly, the nonlinear nature of the interaction can be utilized for an optical amplification of broadband ultrashort laser pulses in a semiconductor-based two-photon laser [Iro92; SB64]. Such a device has several desirable properties, featuring capabilities for efficient ultrafast pulse compression [NHO10b], unique sub-Poissonian photon statistics [Lam67; BEL95] that display, for example, reduced photon noise beyond classical limits [Man79] and a remarkably stable self-mode locking [HFI93].

Despite their promising applications, the realization of these concepts in the solid state environment has remained elusive. Only in recent years, a few groups have reported on stimulated two-photon emission from specific semiconductor structures, e.g. from "artificial atoms" formed by biexcitons in quantum dots embedded in a photonic crystal nanocavity [Ota11] or from electrically pumped AlGaAs waveguides [NHO10a]. Still, one article by *Hayat et al.* [HGO08] claimed the first observation of both spontaneous and singly stimulated two-photon emission from a prototypical bulk semiconductor, being GaAs, in 2008, sparking new interest in the field. However, to the author's awareness, no confirming experimental studies by other groups have been published following up this breakthrough, therefore marking a starting point for this work's experiments presented in Section 3. Also, just recently an experimental paper by *Reichert et al.* [Rei16] shed new light on two-photon emission in bulk semiconductors which demonstrates two-photon gain requiring widely nondegenerate photon configurations that vastly enhance the two-photon optical nonlinearity.

Motivated by these claims, this thesis aims to further the understanding of the two-photon interaction dynamic in bulk direct semiconductors, namely Cu_2O, GaAs and CdSe, in an electronically excited state. A central goal is to asses the practicability of controlling the two-photon transition strength using an ultrafast all-optical scheme and ultimately identify the key parameters and requirements necessary to observe two-photon gain in these media. In the presented experiments, we mostly focus on degenerate two-photon configurations, i.e. we monitor the nonlinear response with both involved photons stemming from a single laser source. This allows us to unambiguously investigate the fundamental excitation-induced modification to both the linear optical and the two-photon coupling at a selected spectral position.

In doing so, this work utilizes several experimental techniques to resolve the phenomenon, starting in Section 3 with a classical spectroscopic approach motivated by [HGO08] in search for stimulated two-photon idler emission signatures, where we subsequently enhance the investigation by ultrafast spectroscopic methods which are able

to directly access both the two-photon coupling strength and carrier-related dynamic within the semiconductor. Section 4 presents a polarization sensitive three-beam approach that allows for a temporal resolution of the two-photon response whilst being able to separate the interplay of carrier-related dynamical effects. Consequently, Section 5 presents the corresponding experimental findings, discusses the related phenomena that occur as a result of the optical excitation and elaborates on the obtained prerequisites to an effective optical control over the two-photon coupling in photoexcited semiconductors.

Part II

Theoretical framework of nonlinear light-matter interaction

2 Introduction to two-photon transitions in semiconductors

Two-photon absorption is a nonlinear optical process which conceptually is easily understandable as a quantum transition to an energetically elevated level that involves the simultaneous annihilation of two photons from an electromagnetic field. Nevertheless, a thorough understanding of the phenomenon requires a deeper insight into the interplay of theoretical concepts from both classical electrodynamics and quantum mechanics that describe this light-matter interaction.

This chapter presents the theoretical foundation to understand two-photon processes in semiconductors, as it is usually presented in common literature [Boy08; Agr89; DC16]. The first section 2.1 illustrates the classical approach to nonlinear light-matter interactions via a nonlinear material polarization that naturally generates a nonlinear absorption process in Section 2.2. While Section 2.3 treats the quantum mechanical descriptions of two-photon transitions, special emphasis on the aspects of two-photon interaction related to the semiconductor medium is given in Section 2.4.

2.1 Classical treatment of nonlinear optics

The propagation of light as it passes through matter is, as is for all electromagnetic phenomena, governed by Maxwell's equations. Within a dielectric medium, the electromagnetic (light-)field $\mathbf{E}$ induces a dipole moment $\mathbf{P}$ between the bound charges of the atomic structure. $\mathbf{P}$ is therefore defined as the dipole moment per unit volume. This material polarization relates to the electric displacement field according to

$$\mathbf{D} = \epsilon_0 \mathbf{E} + \mathbf{P} = \epsilon_0 (1 + \chi_\mathrm{e}) \mathbf{E}, \tag{2.1}$$

where ϵ_0 is the vacuum permittivity. The dielectric susceptibility χ_e connects the incident electromagnetic field to the relative permittivity ϵ_r which models the electronic properties of the material via $\epsilon_\mathrm{r} = 1 + \chi_\mathrm{e}$. In this picture χ_e enters in form of a dimensionless constant, but this relation only holds for the specific case of a homogeneous and isotropic medium with a linear proportionality of the induced polarization to the electric field. It especially breaks down when the anharmonic nature of the atomic Coulomb potential in a solid's structure is taken into account,

where the dense and possibly locally asymmetrical arrangement of atomic nuclei in the periodic solid structure deforms the otherwise parabolic potential.

Therefore, in nonlinear optics, $\mathbf{P}$ is rather described as a power series expansion in the driving electrical field strength

$$\mathbf{P} = \epsilon_0 \sum_{n=1}^{\infty} \chi^{(n)} \mathbf{E}^n \tag{2.2}$$

$$= \epsilon_0 \left(\chi^{(1)} \mathbf{E} + \chi^{(2)} \mathbf{E}^2 + \chi^{(3)} \mathbf{E}^3 + ... \right). \tag{2.3}$$

This circumstance gives rise to a nonlinear response of the medium. The nonlinear susceptibilities $\chi^{(n)}$ are expected to be of successively decreasing magnitude which inversely scales in units of the underlying atomic electric field strength $E_{at} = {}^{e}/_{4\pi\epsilon_0 a_0^2}$, where a_0 is the Bohr radius of the Hydrogen atom, as an example. Hence the lowest order corrections to the linear susceptibility $\chi^{(1)}$ are expected to be on the order of

$$\chi^{(2)} \propto \frac{\chi^{(1)}}{E_{at}} \approx 1.94 \cdot 10^{-12} \frac{m}{V}, \qquad \chi^{(3)} \propto \frac{\chi^{(1)}}{E_{at}^2} \approx 3.78 \cdot 10^{-24} \frac{m^2}{V^2}. \tag{2.4}$$

As a result, higher order terms $\chi^{(n)}$ in the expansion only effectively contribute to the optical polarization $\mathbf{P}$ if the incident light field $\mathbf{E}$ is sufficiently strong, such as the output provided by pulsed laser sources. In effect, the incident light field by this process effectively alters the optical response of the material based on its field strength, what opens additional pathways in light-matter-interaction. This is expressed by the wave equation in an (nonmagnetic, $\mu_r = 1$) optical medium

$$\left(\nabla^2 - \frac{n^2}{c^2} \frac{\partial^2}{\partial t^2} \right) \mathbf{E} = \frac{1}{\epsilon_0 c^2} \frac{\partial^2}{\partial t^2} \mathbf{P}_{NL} \tag{2.5}$$

which couples the nonlinear polarization components $\mathbf{P}_{NL}$ as a driving force to the transmitted electric field, where n is the linear refractive index and c is the vacuum speed of light. By these means the transfer of e.g. amplitude or frequency components between the oscillating nonlinear polarization and the electromagnetic wave is made possible.

Upon describing nonlinear optical phenomena in solid matter, one finds that the susceptibilities $\chi^{(n)}(\omega)$ are frequency dependent, rank (n+1) tensors which express the material's dispersion in the light frequency ω and spatial dimensions x, y or z. For instance, the i-th component of the polarization vector in a second order optical material is formally determined as

$$P_i = \epsilon_0 \left(\sum_{j=1}^{3} \chi_{ij} E_j + \sum_{j,k=1}^{3} \chi_{ijk} E_j E_k \right), \tag{2.6}$$

where the tensor indices i, j, k in the summations correspond to the spatial components x, y, z. As a result, the polarization wave vector inside a medium is not necessarily parallel to the driving field. In solid matter the explicit form of the susceptibility tensor depends on the crystal structure of the material and can be derived from the 32 distinct point symmetry classes that predict which tensor components are non-zero. As a general note, a centrosymmetric material system actually demands all components χ_{ijk} to vanish since the existence of an inversion center conserves the sign of the polarization $\mathbf{P}(t)$ induced by an incident electric field $\mathbf{E}(t)$:

$$-\mathbf{P}(t) = \epsilon_0 \chi^{(2)}[-\mathbf{E}(t)]^2 = \epsilon_0 \chi^{(2)} \mathbf{E}^2(t), \tag{2.7}$$

ergo $\chi^{(2)} = 0$. The same holds true for all even orders of $\chi^{(n)}(\omega)$. Therefore $\chi^{(3)}$, which is relevant to this work, is the lowest-order non-vanishing nonlinearity in any centrosymmetric material and a universal property found in any material regardless of spatial symmetry.

In fact, a rich variety of effects arise from the different orders of $\mathbf{P}$ which are usually referred to in association to their respective order of $\chi^{(n)}$. Firstly, $\chi^{(1)}$ describes linear optical effects via the linear refractive index[1]

$$n = \sqrt{\epsilon_r} = \left(1 + \chi^{(1)}\right)^{1/2}, \tag{2.8}$$

i.e. the refraction, reflection and linear absorption of electromagnetic radiation. The latter emerges from the evaluation of the exact form of ϵ_r: The Lorentz oscillator model describes a dielectric material as an arrangement of positively charged atomic nuclei surrounded by negatively charged electron clouds which can perform harmonic oscillations at the Eigenfrequencies of the system when driven by an external periodic field. As a result, a complex, frequency-dependent dielectric function $\epsilon_r(\omega)$ (cf. eq. (2.1)) governs the material polarization, what results in a complex refractive index

$$\tilde{n}(\omega) = \epsilon_r^{1/2}(\omega) = n(\omega) + i\kappa(\omega) \tag{2.9}$$

with an extinction coefficient $\kappa = \frac{1}{2n} \chi^{(1)}_{Im}$. Upon solving the wave equation (2.5), the imaginary part of $\tilde{n}$ produces an exponential attenuation of the electromagnetic wave $\mathbf{E}$ in space: This results in an absorption of light through a dielectric medium which is described by the Beer-Lambert law for the field intensity I:

$$\partial_z I = -\alpha I \Leftrightarrow I(z) = I_0 \exp(-\alpha z), \text{ with } \alpha = \frac{4\pi\kappa}{\lambda} \tag{2.10}$$

denoting the linear absorption coefficient, λ referring to the optical wavelength and $I_0 = I(z=0)$.

[1] The refractive index is defined as $n = \sqrt{\epsilon_r \mu_r}$. Since the processes described in this work are based on the electric susceptibility χ_e, we restrict the consideration to the case of a nonmagnetic material with $\mu_r = 1$.

More exotic effects arise from higher orders $\chi^{(n)}$. For example, $\chi^{(2)}$ enables effects like optical rectification [Bas62], parametric amplification [Kro62] or second-harmonic generation (SHG) [Fra61], which was the first nonlinear optical effect to be studied by Franken *et al.* in 1961. These higher order processes originate from the coupling of the optical wave to its own light field as well as between several coinciding fields at, for example, different optical frequencies. This is represented in the terms "$\mathbf{E}\cdot\mathbf{E}\cdot..$" present in the polarization expansion given by eq. (2.3).

In order to evaluate these material polarization contributions, both $\mathbf{P}(\mathbf{r},t)$ and the electric field $\mathbf{E}(\mathbf{r},t)$ of the optical wave can be decomposed into a discrete set of infinite plane waves with oscillating frequencies ω_n according to

$$\mathbf{E}(\mathbf{r},t) = \sum_n \mathbf{E_n} e^{-i\omega_n t} + \text{c.c.} \tag{2.11}$$

$$= \sum_n \mathbf{A}(\omega_n) e^{i(\mathbf{k}_n\cdot\mathbf{r}-\omega_n t)} + \text{c.c.} \tag{2.12}$$

where the sum is taken over all positive frequency components ω_n and their complex Fourier amplitudes $\mathbf{A}(\omega_n)$ as well as their complex conjugates. Using this ansatz, the wave equation (2.5) can be solved subsequently. Usually, the slowly varying amplitude approximation (SVAA) is applied which assumes that the longitudinal amplitude and phase variations of the light field are negligible on the scale of the optical wavelength:

$$\left|\frac{\partial^2}{\partial z^2}\mathbf{A}(\omega_n)\right| \ll \left|k\frac{\partial}{\partial z}\mathbf{A}(\omega_n)\right| \tag{2.13}$$

which holds true except for very short optical pulses with only a few electric field cycles and facilitates the calculation of eq. (2.5) by reducing it to a first order differential equation in the propagation direction z. The resultant remaining propagation equation is referred to as the paraxial wave equation

$$2ik_n\frac{\partial \mathbf{A}_n}{\partial z} + \nabla_T^2\mathbf{A}_n = -\frac{\omega_n^2}{\epsilon_0 c^2}\mathbf{P}_n e^{i\Delta kz}. \tag{2.14}$$

On the right hand side, a phase term dependent on the k-vector match between the driving electric field and the polarization response emerges which is of importance to coherent nonlinear optical phenomena such as second-harmonic generation.

On a final note, nonlinear processes can generally be distinguished between parametric and nonparametric processes. A parametric process occurs without energy transfer to or from the medium and is a practically instantaneous response of the system. It can only be described as a virtual excitation during a time interval $\hbar/\delta E$ - Therefore the initial and final state of the system are identical. In general, parametric nonlinearities are always connected to the real part of a susceptibility whilst nonparametric processes are described by complex susceptibilities as it is the case for two-photon absorption.

2.2 The nonlinear refractive index and two-photon absorption law

As stated in section 2.1, the optical nonlinearity of third order $\chi^{(3)}$ is universally observable in condensed matter, regardless of its spatial symmetry. Among a variety of other effects such as four-wave mixing [CCK66] and third harmonic generation [NW67], the third order polarization also leads to a nonlinear index of refraction. This is of key importance to the emergence of two-photon light-matter interaction, as is illustrated in the following.

Given a monochromatic input field for simplicity

$$\mathbf{E}(\mathrm{t}) = \mathbf{E}_\omega \cos(\omega \mathrm{t}) = \frac{1}{2}\mathbf{E}_\omega \, \mathrm{e}^{-\mathrm{i}\omega \mathrm{t}} + \mathrm{c.c.}, \tag{2.15}$$

the optical response of a $\chi^{(3)}$ medium, according to Equation (2.3), is given by

$$\begin{aligned}\mathbf{P}(\mathrm{t}) &= \mathbf{P}^{(1)}(\mathrm{t}) + \mathbf{P}^{(3)}(\mathrm{t}) \\ &= \frac{1}{2}\epsilon_0 \chi^{(1)} \mathbf{E}_\omega \, \mathrm{e}^{-\mathrm{i}\omega \mathrm{t}} + \frac{1}{8}\epsilon_0 \chi^{(3)} \mathbf{E}_\omega^3 \mathrm{e}^{-\mathrm{i}3\omega \mathrm{t}} + \frac{3}{8}\epsilon_0 \chi^{(3)} \mathbf{E}_\omega^2 \mathbf{E}_\omega^* \, \mathrm{e}^{-\mathrm{i}\omega \mathrm{t}} + \mathrm{c.c.}\end{aligned} \tag{2.16}$$

As can be seen, a wave component at the frequency 3ω is generated in relation to $\chi^{(3)}$, which is the aforementioned process referred to as third-harmonic generation (THG). Still, one notices that, additionally, a nonlinear contribution to the polarization field component at the original frequency ω emerges in form of the last term in eq. (2.16). Together with the $\chi^{(1)}$ term, an effective χ_{eff} at the fundamental frequency of the wave can be summarized:

$$\begin{aligned}\mathbf{P}_\omega(\mathrm{t}) &= \mathbf{P}_\omega^{(1)}(\mathrm{t}) + \mathbf{P}_\omega^{(3)}(\mathrm{t}) \\ &= \epsilon_0 \left(\chi^{(1)} + \frac{3}{4}\chi^{(3)} |\mathbf{E}_\omega|^2 \right) \frac{1}{2}\mathbf{E}_\omega \, \mathrm{e}^{-\mathrm{i}\omega \mathrm{t}} + \mathrm{c.c.} \\ &= \epsilon_0 \chi_{\mathrm{eff}} \frac{1}{2}\mathbf{E}_\omega \mathrm{e}^{-\mathrm{i}\omega \mathrm{t}} + \mathrm{c.c.}\end{aligned} \tag{2.17}$$

This allows for a reinterpretation of the refractive index n, when the intensity of the electric field $\mathrm{I}_\omega = \frac{1}{2}\mathrm{c}\mathrm{n}_0\epsilon_0\mathbf{E}_\omega^2$ is introduced:

$$\mathrm{n} = \sqrt{1 + \chi_{\mathrm{eff}}} \simeq \mathrm{n}_0 + \frac{3}{4\mathrm{n}_\mathrm{o}^2\epsilon_0\mathrm{c}}\chi^{(3)}\mathrm{I}_\omega = \mathrm{n}_0 + \mathrm{n}_2\mathrm{I}_\omega. \tag{2.18}$$

For high field intensities I_ω, the refractive index in a $\chi^{(3)}$ medium bears an intensity-dependent contribution n_2. This is referred to as the AC or optical Kerr effect [Sto73] and manifests in form of the cross-phase modulation (XPM) of optical pulses,

soliton formation in fiber optics or the self-focusing of, e.g. Gaussian, intensity profiles in a nonlinear crystal. This has been taken advantage of by the z-scan measurement technique [SSS89] as a popular tool to determine the value of n_2: Here the investigated sample is being moved through the focus of a laser beam which undergoes self focusing/defocusing due to n_2 that can be detected as an intensity variation through an aperture in the beam behind the sample.

Since $\chi^{(3)} = \chi^{(3)}_{\mathrm{Re}} + \mathrm{i}\chi^{(3)}_{\mathrm{Im}}$ can generally be considered as a complex quantitiy, analogous to the complex linear refractive index in eq. (2.9), the imaginary part of the nonlinear index contribution n_2 gives rise to a nonlinear absorption - This is the origin of two-photon absorption (TPA) as the lowest order of multi-photon absorption in the classical picture of the nonlinear polarization. Subsequently, the differential absorption law for the intensity I_ω across a material volume z can be derived from the paraxial wave equation (2.14) for the field amplitude $\mathbf{E}_\omega$:

$$2\mathrm{ik}\frac{\partial \mathbf{E}_\omega}{\partial \mathrm{z}} = -\frac{\omega^2}{\epsilon_0 \mathrm{c}^2}\left(\epsilon_0 \mathrm{n}_0^2 + \frac{3\epsilon_0}{4}\chi^{(3)}|\mathbf{E}_\omega|^2\right)\mathbf{E}_\omega \tag{2.19}$$

$$\Leftrightarrow \frac{\partial \mathrm{I}_\omega}{\partial \mathrm{z}} = -\alpha_0(\omega)\mathrm{I}_\omega - \beta(\omega)\mathrm{I}_\omega^2 \tag{2.20}$$

where the two-photon absorption coefficient β is introduced[2] and defined as

$$\beta(\omega) = \frac{3\pi\chi^{(3)}_{\mathrm{Im}}}{\epsilon_0 \mathrm{n}_0^2 \mathrm{c}\lambda}. \tag{2.21}$$

In effect, a modification to the absorption coefficient α_0 related to $\chi^{(1)}_{\mathrm{Im}}$ as given by 2.10 is thus made in form of a nonlinear correction term related to $\chi^{(3)}_{\mathrm{Im}}$,

$$\alpha(\omega) = \alpha_0(\omega) + \beta(\omega)\mathrm{I}. \tag{2.22}$$

The solution to eq. (2.20) yields the two-photon absorption law for a single input field

$$\mathrm{I}(\mathrm{z}) = \frac{\mathrm{I}_0\,\mathrm{e}^{-\alpha_0 \mathrm{z}}}{1 + \frac{\beta}{\alpha_0}\mathrm{I}_0(1 - \mathrm{e}^{-\alpha_0 \mathrm{z}})} \overset{\alpha_0 \to 0}{=} \frac{\mathrm{I}_0}{1 + \beta(\omega)\mathrm{I}_0 \mathrm{z}} \tag{2.23}$$

with $\mathrm{I}_0 = \mathrm{I}(\mathrm{z} = 0)$ being the intensity entering the front facet of the medium. The linear absorption α_0 may not necessarily stem from direct absorption of photons (which does not occur for photon energies below the bandgap energy E_g of a given semiconductor), but can also originate from photon scattering processes of linear order such as free carrier absorption [Pid80].

[2] In some literature the nonlinear absorption coefficient is stated as $\alpha_2(\omega)$ instead of $\beta(\omega)$, what emphasizes the second order correction in electrical field strength $\mathbf{E}^2$ made to the refractive index.

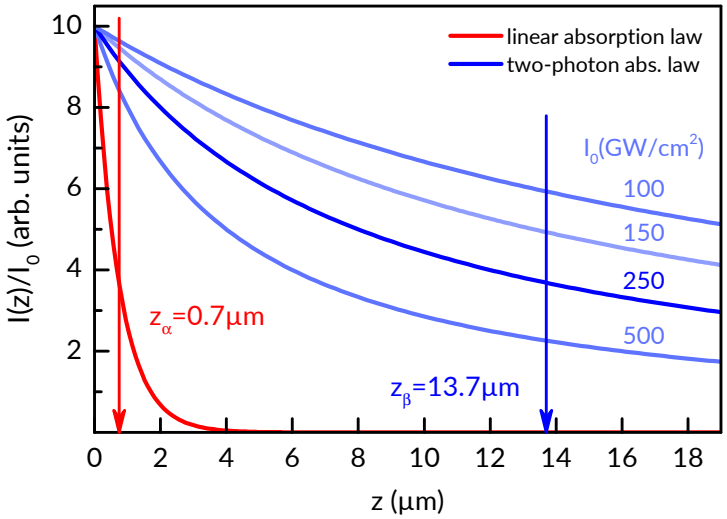

Figure 2.2.1: Model comparison of the optical absorption profile in linear optics and two-photon absorption in nonlinear optics. The red curve represents the Lambert law (2.10) while the blue curves represent the TPA law (2.23) for various power densities I_0 typical for a fs-pulsed laser. GaAs model parameters are used, i.e. $\alpha_0(1.55\,\mathrm{eV}) = 13455\,\mathrm{cm}^{-1}$[Asp86] and $\beta(0.78\,\mathrm{eV}) \simeq 5\,\mathrm{cm/GW}$[Kri11].

Figure 2.2.1 illustrates the absorption profiles of a generic 50 fs, 200 kHz modulated laser pulse in either a medium with direct absorption of single photons as described by the Lambert law (2.10) or two-photon absorption according to (2.23) arising from the nonlinear refractive index in the otherwise transparent wavelength region of the material. Absorption parameters for an optical transition at Ti:sapphire photon energies for bulk GaAs are referred to as a prototypical example. As can be seen by the red line, direct absorption produces a rapid, exponential attenuation of the laser intensity with typical penetration depths $z_\alpha = \alpha^{-1} \sim .7\,\mu\mathrm{m}$ of several hundreds of nanometers into the material. Here, while addressing the same energetic states, two-photon absorption, in form of the blue lines, on the other hand penetrates the sample on a ten-micrometers scale ($z_\beta = (\beta I_0)^{-1}$) due to it being a weaker, third order process. Furthermore, the dependence on strong irradiance in the order of several $\mathrm{GW/cm^2}$ to produce noticeable absorption is evident. In the given example, a laser pulse with $I_0 = 50\,\mathrm{mW}$ is focused to 50 µm spotsize. If one were to use a continous wave laser source, the resultant two-photon absorption in a 1 cm thick sample would only amount

$$\Delta I_{cw} \simeq -1.3 \times 10^{-5}\, I_{cw}.$$

These considerations show that transient two-photon signatures outside of ultrafast optics are vanishingly small, but also suggest two-photon absorption as a tool for optical excitation of deeper layers of a bulk semiconductor in a pump-probe scheme.

2.3 Quantum theory of semiconductor two-photon interaction

In order to describe two-photon processes and correctly assess the two-photon coupling terms expressed in the $\chi^{(3)}$ tensor, a microscopical description of the underlying dispersion within a quantum mechanical picture is necessary. A two-photon transition may both function as an absorption (TPA) or emission (TPE) process which involves two quanta of the electromagnetic field, or photons, simultaneously in a single electronic transition. Similar to single photon transitions, TPA may occur as the annihilation of said two photons which elevates the system from its ground into an excited state, whereas TPE manifests as the emission of a photon pair from an electronic deexcitation in form of either a spontaneous process or a stimulated transition invoked by one or two external fields. As an obvious extension to linear light absorption, most scientific works foremost focus on analyzing the process of two-photon absorption, albeit the applied considerations can easily be transfered to TPE. An introduction to the central theoretical aspects of quantum two-photon models and the key insights gained from these theories is presented in the following.

The first approach to multi-photon processes has been done in 1927 by P. Dirac [Dir27] when he published a quantum theory of dispersion for the interaction of a quantized electromagnetic field and an atomic system within the Hamiltonian formalism. Based on this formalism, M. Göppert-Mayer firstly published a fundamental theoretical description of atomic two-photon processes in her dissertation "Über Elementarakte mit zwei Quantensprüngen" from 1931 [Göp31]. The theoretical tool used in the research by Dirac and Göppert-Mayer is commonly referred to as perturbation theory and has been widely adopted by the scientific community in the effort of developing a semiconductor-based two-photon absorption theory.[3]

The key idea is to calculate the probability for an electron to undergo the transition from its inital (ground) state into an energetically elevated (excited) state when the steady-state system Hamiltonian H_0 is accompanied by a comparatively weak perturbation, in this case by the electron-radiation interaction Hamiltonian in dipole approximation:

$$\hat{\mathrm{H}}_{\mathrm{opt}} = -\frac{\mathrm{e}}{\mathrm{m}_0}\hat{\mathbf{A}}\cdot\hat{\mathbf{p}} = \frac{\mathrm{e}}{\mathrm{im}_0\omega}\left(\frac{2\pi\mathrm{I}}{\mathrm{n}_0\mathrm{c}}\right)^{1/2}\hat{\mathbf{e}}\cdot\hat{\mathbf{p}}. \tag{2.24}$$

[3] Historically, L.V. Keldysh later introduced another formalism able to derive multi-photon absorption coefficients that is based on tunneling rate calculations of dressed electronic wave functions in an AC light field [Kel65]. Although predicting the correct scaling laws, this theory fails to incorporate more elaborate semiconductor models that later were found to yield dominant contributions to the TPA process, e.g. band degeneracies which expand the possible intraband transitions [HS92].

Here $\mathbf{A}$ is the vector potential operator (in Coulomb gauge) representing the oscillating light field with $\hat{\mathbf{e}}$ being the polarization unit vector and the electron momentum operator $\hat{\mathbf{p}}$.

The two-photon transition rate W_2 resulting from this weak coupling is expressed by Fermi's Golden Rule in second order for a time-dependent perturbation [Wei81; Whe84]:

$$W_2 = \frac{2\pi}{\hbar} \sum_{vc} \left| \sum_{i} \frac{\langle \phi_c | \hat{H}_{opt} | \phi_i \rangle \langle \phi_i | \hat{H}_{opt} | \phi_v \rangle}{E_i(\mathbf{k}) - E_v(\mathbf{k}) - \hbar\omega} \right|^2 \delta(E_{cv}(\mathbf{k}) - 2\hbar\omega). \tag{2.25}$$

The notation in eq. (2.25) already caters to the specific case of two-photon transitions in the semiconductor medium: In contrast to two-photon transitions in discrete-level atomic systems, instead of localized atomic states here delocalized electron Bloch wavefunctions $\phi(\mathbf{k})$ with crystal momentum $\mathbf{k}$ have to be considered. Due to the Pauli-exclusion principle the periodic many-particle structure of the solid state forces the electron quantum states into a series of bands in k-space with quasi-continuous dispersion. In the case of an intrinsic semiconductor, the highest occupied band in thermal equilibrium, called the valence band (v), is offset from the lowest unoccupied band, named conduction band (c) by the bandgap energy E_g ($=E_{cv}(0)$ in a direct semiconductor), cf. Figure 2.3.1. The two photons which stimulate an electron transition $|\phi_v\rangle \rightarrow |\phi_c\rangle$ therefore need to posses at least a sum energy of E_g, i.e. $E_g/2 \leq \hbar\omega < E_g$ to bridge the required energy difference between both band states.

As can be seen from Equation (2.25), the calculation of the two-photon transition rate W_2 for a given state separation energy E_{cv} requires the summation over all eligible filled states $|\phi_v\rangle$ in the valence band and empty states $|\phi_c\rangle$ in the conduction band. Intrinsically, the two-photon transition occurs via a sum over all possible intermediate states $|\phi_i\rangle$. These are no resonant eigenstates of the quantum system, but arise from the light field perturbation only to mediate the quantum transition process. Hence they are referred to as virtual states and possess an uncertainty lifetime $\hbar/\Delta E$. Ultimately, the delicate part about the calculation of W_2 is the choice of an appropriate band structure model to define the distribution and dispersion of the participant states.

A common band structure model consists of a set of parabolic valence and conduction bands with band extrema at the center of the Brillouin zone and hence mirrors a direct gap semiconductor. This type of model has become known as the Kane model [Kan57]. Here one generally distinguishes between allowed and forbidden quantum transitions within dipole order of the electron-radiation interaction $\hat{H}_{opt}$. A forbidden transition is generally suppressed in probability, since it requires higher order (quadrupole etc.) interaction matrix elements. On the other hand, an interband transition between the

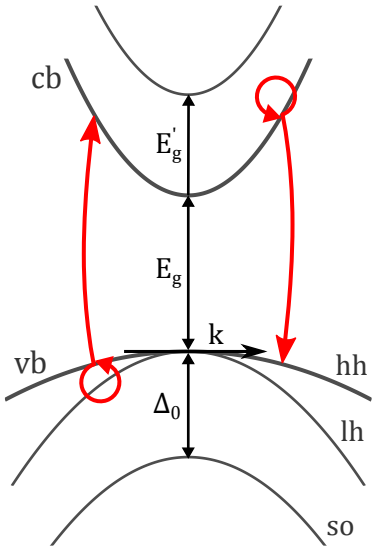

Figure 2.3.1: Kane band structure model consisting of the lowest two conduction bands (offset from the valence band by the bandgap energies E_g and E_g') and the degenerate heavy-hole (hh), light-hole (lh) and split-off (so) valence bands. For a two-band model consisting of single valence band (vb) and conduction band (cb), the two possible forbidden-allowed transitions involving a combined intraband self-scattering process and a interband transition are shown in red.

typically p-type valence and s-type conduction band[4] is an allowed transition since it transfers the photon angular momentum $\hbar$, while an intraband transition of an electron state in, for example, the valence band is of forbidden type when coupled to a photon in the dipole interaction framework. In a two-band model consisting of just one conduction and valence band each, the intermediate states $|\phi_i\rangle$ are states at $\mathbf{k} \neq 0$ within the bands themselves. therefore the two-photon transitions that enter the calculation of W_2 are combined allowed-forbidden transitions. The resultant two-photon absorption coefficient for a single beam is then given by [HW94]

$$\beta(\omega) = K \frac{\sqrt{E_p}}{n_0^2(\omega) E_g^3} F_2\left(\frac{\hbar\omega}{E_g}\right), \quad F_2(x) = \frac{(2x-1)^{3/2}}{(2x)^5} \text{ for } 2x > 1. \tag{2.26}$$

This is a universal notation of $\beta(\omega)$ whose explicit value depends on the form of its constituent model parameters. In detail, the factor E_p comprises the interband momentum matrix element and thus in the parabolic model is defined by $E_p = 2|\mathbf{p_{vc}}|^2/m_0$. For most semiconductors this is in fact an almost constant value $E_p \simeq 21\,\text{eV}$ [Kan80]. As mentioned before, E_g represents the material band gap and n_o

[4] The s- and p-type notation here refers to the constituent atomic orbital wave functions forming the respective electronic band near the Γ-point ($\mathbf{k}=0$) which define its orbital momentum and symmetry [Gru16] (pp. 26-31).

the optical refractive index. Their predicted scaling behaviour ($n_o^{-2}E_g^{-3}$) has been confirmed over a large range of semiconductors and wide-gap optical materials [Whe84; Str85] and allow for a determination of the TPA magnitude. The Kane parameter K is a material independent coupling parameter that depends on the underlying band structure model. Historically, measured discrepancies to the two-band model have been overcome by fitting this constant to the experimental data which has given a value of $K_p = 3100\,\mathrm{cm/GW\,(eV)^{5/2}}$ [Str85]. The dispersion of the two-photon coefficient $\beta(\omega)$ is predicted by the spectral function F_2. It is found that the transition strength near the two-photon band edge grows strongly due to the increasing density of sates but eventually levels off at higher energies, when the denominators in eq. (2.25) dominate the quantum transition amplitudes.

While the two-band model already provides a good qualitative description for the band-edge optical properties of direct semiconductors, where it produces some universal scaling dependencies, some important aspects need to be added to the the model to describe all relevant phenomena. First off, the band fine structure in form of a three-times valence band degeneracy needs to be accounted for: The valence band at the center of the Brillouin zone is a p-type state with orbital momentum $\mathbf{L} = 1$ and thus consists of three individual bands: the two degenerate light-hole (lh, $J_z = 1/2$) and heavy-hole (hh, $J_z = 3/2$) bands with a total angular momentum $\mathbf{J} = \mathbf{L} + \mathbf{S} = 3/2$, as well as a split-off band for $\mathbf{J} = 1/2$ which is separated by the spin-orbit interaction energy Δ_0. These add more possible forbidden-type intervalence band transitions that substantially enhance the two-photon coupling [Pid79]. To further develop a quantitative semiconductor two-photon theory, a more sophisticated description of the off-center electronic wave functions and band non-parabolicities [Wei81], as well as the inclusion of excitonic contributions [LF74] for near-edge transitions have been included.

So far the described two-photon absorption process accounts to a degenerate case where the two photons involved are of identical frequency, polarization and source. While the experiments presented in this thesis rely on a single photon source, the three-beam configuration in Chapter IV explicitly investigates TPA between two separate light inputs with alterable polarization. Most importantly, here the absorption process between two crossed linear polarizations couples the x- and y-components (w.l.o.g.) of both optical polarization fields. It is therefore mitigated by the offdiagonal elements of the $\chi^{(3)}$ tensor that contribute to the two-photon coefficient (for two frequency-degenerate fields) via

$$\beta(\omega) = \frac{3}{2}\frac{\omega}{\epsilon_0 n_0^2 c^2}\left[\chi''_{xxxx}\Sigma + 2\,\chi''_{xyxy}(1-\Sigma) + \chi''_{xxyy}(|\hat{\mathbf{e}}\cdot\hat{\mathbf{e}}|^2 - \Sigma)\right], \tag{2.27}$$

with the polarization parameter $\Sigma = \Sigma_r|e_r|^4$ and $\chi''_{xyxy} = \mathrm{Im}\,\chi^{(3)}_{xyxy}(-\omega,\omega,\omega)$, etc. [HW94]. A polarization anisotropy in these diagonal elements does not occur in an

isotropic two- or four-band model, but stems from contributions of higher bands, especially the nearest higher conduction band [Dvo94], cf. Figure 2.3.1. This band typcially lies a few eV above the conduction band minimum (at a gap energy E_g') and, in a zincblende semiconductor, has the same symmetry class (Γ_{15}) as the valence band what enables allowed-type intermediate transitions to this band as a symmetry operation of the noncentrosymmetric crystal structure. In general, the corresponding momentum matrix elements for a transition between the valence band wavefunctions $|X\rangle$, $|Y\rangle$ and $|Z\rangle$ to the higher band states $|X'\rangle$, $|Y'\rangle$ and $|Z'\rangle$ are

$$\langle X'|\, p_y\, |Z\rangle = \langle Y'|\, p_z\, |X\rangle = \langle Z'|\, p_x\, |Y\rangle = -\frac{im}{\hbar}\, Q, \tag{2.28}$$

whilst on the other hand, a subsequent transition to the s-like conduction band state $|S\rangle$ is defined by the matrix elements

$$\langle X'|\, p_x\, |S\rangle = \langle Y'|\, p_y\, |S\rangle = \langle Z'|\, p_z\, |S\rangle = -\frac{im}{\hbar}\, P'. \tag{2.29}$$

Here Q and P' are the respective band coupling parameters analogous to the Kane Parameter K introduced before. As can be seen, a transition sequence involving the higher conduction band here incorporates two photons in different polarization states. As an example, a transition from the $|Z\rangle$ valence band state to the $|S\rangle$ state requires both field components E_y and E_x.

Nevertheless, the dominant contribution to the polarization anisotropy in two-photon absorption, according to [Dvo94], rather results from the mixing of the higher band wavefunctions into the valence band states at $|\mathbf{k}| > 0$ than an allowed-type intermediate transition. Such an off-center, perturbed valence state $|Z\rangle$ is described by $\mathbf{k}\cdot\mathbf{p}$ perturbation theory to denounce

$$|Z\rangle \simeq |Z\rangle - \frac{ik_z P}{E_g}\, |S\rangle - \frac{iQ}{E_g'}\left(k_x\, |Y'\rangle + k_y\, |X'\rangle\right). \tag{2.30}$$

Taking the forbidden-allowed transition from $|Z\rangle$ to $|S\rangle$, as illustrated in Figure 2.3.1, into consideration, the polarization anisotropy becomes evident: Since the allowed interband transition in this case requires $\hat{z}$-oriented polarization, the forbidden-type self-scattering process of an identically polarized photon occurs via the second term in eq. (2.30), while a cross-polarized two-photon transition involves the third term. Albeit the higher band mixing enables cross polarized two-photon absorption processes, it does so at a suppressed amplitude $\sim 1/E_g'$. Subsequently, an anisotropy parameter σ has been estimated by *Dvorak et al.* to

$$\sigma^{\text{theory}} = -\frac{2\chi_{xyyx}^{\text{aniso}}}{\chi_{xxxx}^{\text{iso}}} \sim -\frac{2E_g}{E_g'} \tag{2.31}$$

which they experimentally verified in GaAs and CdTe at a wavelength of 950 nm, where they measured parameter values of -0.76 and -0.46.

2.4 The semiconductor based two-photon gain mechanism

Since this thesis investigates the optical control over two-photon absorption, the theoretical description of the two-photon process outlined in Section 2.3 has to be expanded further to incorporate an optical excitation. The central idea is to take advantage of the symmetry in the two-photon transition matrix element $\boldsymbol{\mu}$ in eq. (2.25) regarding the choice of initial states $|\mathrm{i}\rangle$ and final states $|\mathrm{f}\rangle$, i.e.

$$\boldsymbol{\mu} = \sum_{\mathrm{n}} \frac{\langle \mathrm{f}| \, \hat{\mathbf{e}} \cdot \hat{\mathbf{p}} \, |\mathrm{n}\rangle \, \langle \mathrm{n}| \, \hat{\mathbf{e}} \cdot \hat{\mathbf{p}} \, |\mathrm{i}\rangle}{\mathrm{E_f} - \mathrm{E_n} - \hbar\omega_\mathrm{p}}. \tag{2.32}$$

Other than constructing a transition from an equilibrium ground (valence) state to an excited (conduction) state via the absorption of a photon, one can prepare the system in an excited state and perform a deexcitation to the ground state driven by light interaction at the same coupling amplitude. As a result, instead of annihilating a photon from the light field during both two-photon transition steps, a quantum is being added to the field and coherently emitted from the deexcitation. This process is referred to as stimulated two-photon emission and effectively serves as a gain mechanism for the irradiated light intensity.

Within semiconductor laser theory the occupation probability of the two-photon resonant band states can be described by the nonequilibrium Fermi-Dirac distributions given by

$$\mathrm{F_{v/c}}(\mathbf{k}) = \left(\exp\left[(\mathrm{E_{v/c}}(\mathbf{k}) - \mathrm{E_{F_{v/c}}})/\mathrm{k_B T}\right] + 1\right)^{-1} \tag{2.33}$$

with the Boltzmann constant $\mathrm{k_B}$, the band state energy levels $\mathrm{E_v}(\mathbf{k})$ and $\mathrm{E_c}(\mathbf{k})$ and the respective quasi Fermi levels $\mathrm{E_{F_v}}$ and $\mathrm{E_{F_c}}$. Here the latter identify the electronic state population levels within each band. Within a low-temperature approximation, where the Fermi-Dirac distribution approximates a step function, these can be interpreted as the highest occupied electron energy levels within one band. An approach to the calculation of $\mathrm{E_{F_{v/c}}}$ is presented in Section 5.3. With the help of these distribution functions the summation over initial band states in Equation (2.25) can be transformed into a k-space integral weighed by a Fermi occupation factor $[\mathrm{F_c}(\mathrm{k}) - \mathrm{F_v}(\mathrm{k})]$. Given the quasi-Fermi levels are known, this factor determines the magnitude and sign of the two-photon transition rate for an energy $\mathrm{E_{fi}}$. The net two-photon transition rate M then takes the form of [HNO09]

$$\mathrm{M} = \frac{2\pi}{\hbar}\left(\frac{4\pi^2 \mathrm{e}^4 \mathrm{I}^2}{\mathrm{n_p c^2 m^4 \omega_p^4}}\right) \sum_{\mathrm{f}} \int_{-\infty}^{\infty} |\boldsymbol{\mu}|^2 \left[\mathrm{F_c}(\mathbf{k}) - \mathrm{F_v}(\mathbf{k})\right] \times \delta(\mathrm{E_{fi}} - 2\hbar\omega_\mathrm{p}) \, \frac{\mathrm{d}\mathbf{k}}{(2\pi)^3}. \tag{2.34}$$

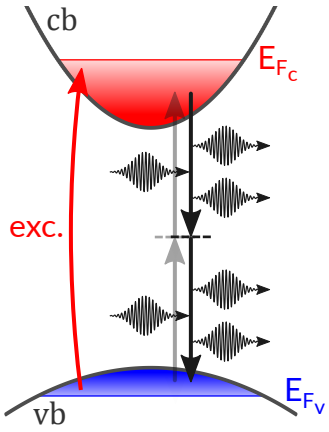

Figure 2.4.1: Illustration of the semiconductor based two-photon gain mechanism. An excitation of the material leads to an occupation of states in the conduction band (up to E_{F_c}) that act as initial levels of the two-photon quantum transition. Subsequently, stimulated emission instead of absorption takes place for photons with an energy $E_g/2 < \hbar\omega_p \leq (E_{F_c} - E_{F_v})/2$.

For the case of an unexcited semiconductor, there is no occupation of conduction band states in thermal equilibrium and therefore M is negative, what indicates an absorption process. In the case of an excited semiconductor, conduction band states up to E_{F_c} are filled with electrons that may deexcite to empty valence band states down to E_{F_v}. In effect, this reverses the sign of the matrix element M for two-photon transitions within the quasi-Fermi energy separation interval $E_g \leq 2\hbar\omega_p \leq \Delta E_F = E_{F_c} - E_{F_v}$.

In order to generalize the two-photon coefficient to incorporate the band state occupation, semiconductor laser theory formulates a net semiconductor two-photon gain coefficient γ_2 [Iro92] stated as

$$\gamma_2(\omega_p) = (2\hbar\omega_p/I^2)\,M. \tag{2.35}$$

Within a typical two-photon experiment the excitation of a sample material is not homogenous accross the sample depth, as well as the ultrafast pulses undergoing two-photon absorption do cover a notable spectral range. Therefore γ_2 usually reveals a continuous trend under excitation that reflects the sample two-photon gain as a whole.

Part III

Pump-probe approach to singly stimulated two-photon emission in Cu_2O and GaAs

3 Single Beam Experiments in Cu_2O and GaAs

This chapter presents introductory experiments on room-temperature two-photon absorption (TPA) and emission (TPE) in bulk semiconductors. At first, Section 3.1 reports the earliest published experimental evidence of semiconductor-based stimulated TPE and discusses the central features of the specific nondegenerate detection scheme. While Section 3.2 introduces our experimental setup and the investigated samples in singly stimulated two-photon experiments, we both present a spectroscopic approach to stimulated two-photon idler emission in Section 3.3 and a direct study on the impact of an optical excitation on bulk TPA by means of an ultrafast spectroscopy method in Section 3.4.

3.1 Motivation for bulk room temperature stimulated TPE

The first experimental evidence for stimulated two-photon emission from bulk semiconductor devices has been reported by *Hayat et al* in 2008 [HGO08]. In this work, the authors have spectrally resolved the room-temperature photoemission of a ∼200 µm thick bulk GaAs sample using an IR femtowatt photoreceiver in combination with a grating monochromator placed in the transmission direction of the sample.

In order to optically pump the sample, the authors applied a 100 mW green continuous wave (cw) Ar-Laser at 514 nm (1.73 eV) to the sample. In the process, an estimated electron-hole density of $n_e \sim 1.2 \times 10^{18}\,\mathrm{cm}^{-3}$ has been injected into the sample within the laser penetration depth on the order of $z \simeq 100\,\mathrm{nm}$. As a result of carrier recombination, they have detected a continuous, spectrally wide near-IR emission signal with a total collected optical power of $\sim 3\,\mathrm{nW}$ using a lock-in scheme. The authors attribute this signal to a homogeneously broadened spontaneous two-photon emission process with a wide maximum at half the one-photon transition energy of the electron-hole recombination, which they experimentally determine to be either 0.82 eV (cf. Figure 3.1.1), or 0.84 eV for the case of an elevated excitation density $n_e \sim 2 \times 10^{18}\,\mathrm{cm}^{-3}$. When compared to the room-temperature bandgap energy of bulk GaAs, which denotes $E_G = 1.42\,\mathrm{eV}$ [Mad04] and defines the one-photon excitation energy required in an equilibrium semiconductor, this result indicates a substantial shift in the electron Fermi energy of at least $\Delta E_F \geq 220\,\mathrm{meV}$ caused by the electron-hole excitation.

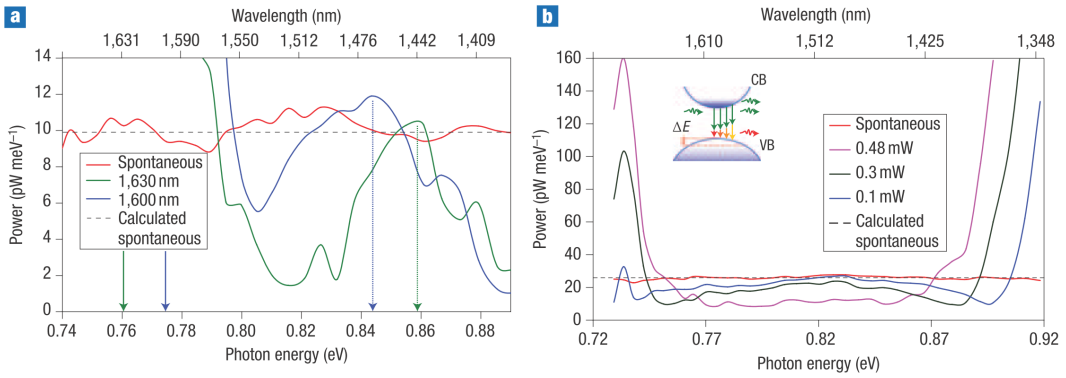

Figure 3.1.1: Bulk GaAs TPE measurements and calculations with optical pumping by a 514-nm Ar laser. a, Spontaneous and singly stimulated TPE, using a 100-mW pump, at different wavelengths and with 0.2-mW stimulation power. The solid arrows indicate the stimulating photon energies and the dotted arrows indicate the theoretical stimulated photon central energies. **b,** Spontaneous and singly stimulated TPE, using a 180-mW pump, with various stimulation powers at 1,310 nm. The inset is a schematic description of singly stimulated TPE energy broadening in a bulk semiconductor. Figure adapted with permission from [HGO08].

In the same study, the authors aim to demonstrate stimulated two-photon emission from the optically excited GaAs sample by irradiating a second 0.2 - 0.48 mW stimulating cw laser with photon energies close to the spontaneous TPE maximum. Due to energy conservation within the two-photon transition, a spectral offset from the spontaneous two-photon maximum in the photon energy of the stimulating laser is expected to produce a complementary idler emission peak centered at an energy $\hbar\omega_{\mathrm{idl}} = 2\,\hbar\omega_{\mathrm{spont}} - \hbar\omega_{\mathrm{stim}}$ which comprises the co-emitted photons during the stimulated two-photon electron-hole recombination, so the authors claim. Indeed, the authors present measurements revealing potential idler peak signatures in their recorded emission spectra, as referenced in Figure 3.1.1. They find that the co-emission of idler photons is accompanied by a decreasing level of spontaneous two-photon emission, but appears as a signature of comparable strength to the spontaneous TPE background in the results presented in figure 3.1.1**a**. In order to validate the signature's origin as stemming from a two-photon process, *Hayat et al.* demonstrate linear gain in the idler amplitude upon increasing the stimulation intensity, as shown in Figure 3.1.1**b**, producing pronounced peak signatures an order of magnitude ($\mathrm{P_{idl}} = 160\,\mathrm{pW/meV}$) in power above the spontaneous background intensity. As a result, the authors detect an idler photon emission up to an estimated total power of 2.4 nW as a result of the stimulation with 0.48 mW infrared pulses after optical excitation of the sample.

To comment on the presented results, we would expect the spectral idler peak bandwidth $\Delta\hbar\omega_{\mathrm{idl}}$ to be proportional to the carrier-energy distribution available

for the stimulated two-photon emission process, same as the spectral profile of the stimulating laser. Surprisingly, an idler bandwidth of a mere $\Delta E_{idl} \simeq 12\,meV$ (FWHM) can be deduced from the presented spectrain Figure 3.1.1**b**. Here one would expect a notably wider profile, since each emitted photon pair originates from a stimulated two-photon transition event where the idler photon energies reflect the electron-hole occupation distribution since the signal photons are fixed in energy by the stimulating narrow-band cw laser. However, $\Delta\hbar\omega_{idl}$ is an order of magnitude smaller than the previously determined Fermi energy shift inferred from the spontaneous TPE maximum. This figure acts as an indicator of the electronic band occupation level relative to the band gap energy that is able to partake in a recombination event and therefore contributes to the TPE broadening, as illustrated by the inset in fig. 3.1.1**b**.

In itself, the here observed Fermi energy shift ΔE_F seems remarkably large and is unlikely be produced by carrier densities $n_e \leq 2\times10^{18}\,cm^{-3}$ in bulk GaAs. Our own estimations predict this value in the vicinity of $\Delta E_F \simeq 70\,meV$. Since the experiments here have been conducted at room temperature, a temperature dependent shift of the sample bandgap energy to higher energies can be ruled out as a potential explanation.

In summary, the here reported appearance of spectral idler signatures complementary to a two-photon resonant stimulation laser pulse in an optically excited semiconductor displays the expected dependencies regarding the emitted photon energy and stimulation intensity, but at the same time reveals unintuitive behaviour in terms of the spectral idler bandwidth and energy offset to the optical bandgap. For us in order to gain more insight into the stimulated two-photon emission process and to explore its properties, the presented measurement principle serves as a starting point for the following two-photon experiments.

3.2 Measurement principles

In the following, the measurement setup employed for the investigation of singly stimulated TPE, as it is depicted in Figure 3.2.1, is outlined. As a basic principle, our optical setup utilizes a pump-probe configuration where two separate laser beams consisting of ultrashort modelocked pulses perform an excitation of the sample via the so-called pump beam whilst simultaneously monitoring the optical response in the probe beam. This is achieved by a tunable variation in the relative arrival time at the sample between both pulse sets achieved by an optical path delay to, in our case, the probe beam.

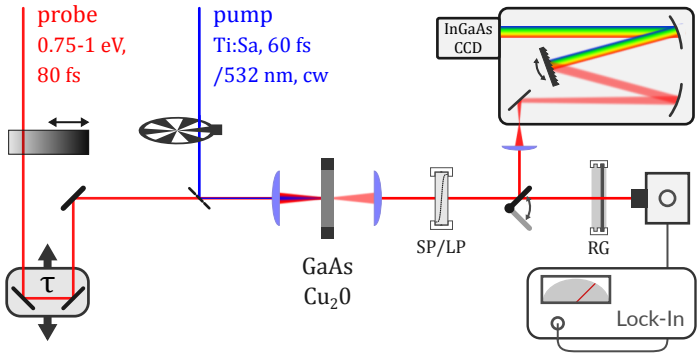

Figure 3.2.1: Outline of the optical setup for room temperature stimulated TPE experiments. Utilizing a pump-probe scheme, an infrared probe laser undergoes weak two-photon absorption in a direct semiconductor sample following a pump laser excitation. Both a spectroscopic and a lock-in detection scheme for the transmitted probe pulses are at hand.

In our experiment, the optical excitation by means of the pump beam can be performed by either a 250 kHz Titanium Sapphire Laser that emits 1.55 eV pulses with 60 fs duration for time-resolved measurements or a green continuous wave (cw) laser source, as it is the case for the experiment in [HGO08]. Both systems are capable to induce the required carrier densities $n_e \sim 10^{18}\,cm^{-3}$ to yield two-photon emission as it has been reported by *Hayat et al.* As for the probe beam, spectrally tunable pulses in the range from 0.75 eV to 1 eV with an effective 80 fs duration address the two-photon absorption of the sample material of choice and are monitored in planar transmission through the sample. To perform intensity dependent measurements, the probe beam can be attenuated using a motorized linear filter. A more detailed description of the laser sources will be given in Section 4.2, where a second experimental setup is presented. To achieve the power densities required for nonlinear optical interactions, both beams are focused onto the sample with a spot diameter of 50-200 µm for the pump and 20-50 µm for the probe beam.

Behind the sample two detection schemes are available. A grating spectrometer with 2 nm resolution combined with a cooled (in order to reduce dark counts) InGaAs detector array is used for spectrally resolved measurements presented in the following Section 3.3. In this configuration, additional short- and long pass filters are placed in the probe beam to prevent residual pump and probe light from entering the spectrometer upon investigating potential idler signatures stemming from stimulated TPE.

By means of a flippable mirror we are able to switch to the detection of the total transmitted probe intensity via an InGaAs photodiode. In front of the diode, an RG1000 long pass filter suppresses any residual pump light that may disturb the probe detection. Here it is possible to both detect the DC probe photocurrent as well as an AC probe modulation which is induced by the mechanically chopped pump beam. This AC pump-probe signal is isolated by a Lock-In detector referenced to the chopper frequency and represents the optical response to the sample excitation including its two-photon absorptivity.

Concerning the investigated semiconductor samples, we here study GaAs as a prototypical nonlinear material in analogy to the published reports on stimulated two-photon emission in [HGO08]. GaAs is a direct III-V semiconductor with zincblende structure and a room temperature (300 K) Γ-point band gap at 1.424 eV [Mad04]. Therefore, the optical pump lasers used in our experiments (emitting sub-871 nm light) undergo linear absorption with little penetration depth well above the band edge of the GaAs sample. Both an 800 nm thin epitaxial GaAs layer in (100) crystal orientation and a macroscopic (111) oriented sample with 500 µm thickness are used in our experiments. Furthermore, Cu_2O, or copper(I) oxide, has been chosen as a second direct semiconductor with cubic crystal structure for investigation. Cu_2O is a prominent spectroscopic material due to its exotic band configuration at the Γ-point, where the lowest conduction band and top (lh) valence band have the same parity, since the valence band here is dominated by Cu 3d states [Ito98]. This effectively prohibits optical transitions of electric-dipole order near the direct bandgap, but allows for nonlinear processes[1] in this regime. Historically, Cu_2O has been of primary spectroscopic interest due to its strong excitonic binding resulting in a high excitability of these quasi-atomic bound electron-hole pairs and small recombination line widths at cryogenic temperatures [Kaz14]. Still, Cu_2O's nonlinear optical properties have also been well studied, especially in relation to two-photon absorption [SRG14; FRW87]. For our experiments, we use a (100) oriented crystal with 500 µm thickness.

[1] Due to the centrosymmetric crystal structure of $Cu_2(I)O$, the lowest nonlinear polarization contribution is of $\chi^{(3)}$ order, as it is required for two-photon processes.

3.3 TPE-idler generation experiments

As presented in Section 3.1, the generation and detection of idler photons from an electronic deexcitation driven by the irradiation of a signal light field which is tuned to a nondegenerate two-photon transition, i.e. involving two photons at different energies, is reportedly suitable for studying stimulated two-photon emission processes in a bulk semiconductor. Before presenting our experimental findings, the experimental principle is reiterated in the following.

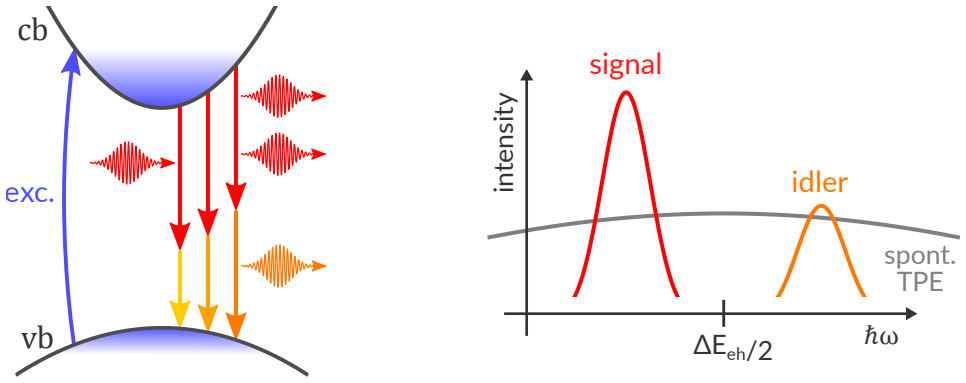

Figure 3.3.1: Schematic depictions of a singly stimulated nondegenerate TPE experiment. In an electronically excited semiconductor, a signal laser pulse generates an energetically broadened two-photon idler pulse by driving the electron-hole recombination. Hereby, the detuning of the idler spectrum from the spontaneous TPE central energy $\Delta E_{eh}/2 \approx E_g/2$ is defined by sum energy conservation with the signal photons.

As depicted in Figure 3.3.1, an excitation of the semiconductor material leads to the population of electronic states in the conduction band (cb) and hole states in the valence band (vb) which are able to radiatively recombine within the carrier lifetime specific to the given material. Besides the emission of luminescence radiation with photon energies near the direct bandgap E_g, also multiphoton processes, such as spontaneous TPE, are involved in the deexcitation. By irradiating photon pulses at a fixed energy below the bandgap, referred to as the signal (illustrated red), one aims to selectively drive the two-photon mediated recombination. Thereby, a stimulated emission process takes place for the signal photons in which additional idler photons are emitted that satisfy the sum energy condition $\hbar\omega_{idl} + \hbar\omega_{sig} = E_{eh} \approx E_g$ for the electron-hole recombination of carriers near the bandgap energy E_g. Since the signal laser pulse has a limited spectral width, any additional spectral width of the idler peak then reflects the carrier energy distribution ΔE_F for electronic states that provide a population inversion for the stimulated TPE process, cf. Section 2.4.

In order to identify a spectral corridor for the emission of idler photons from a two-

photon process we first aim to gain insight into the electronic structure of our samples by identifying the photoemission energy from spontaneous optical recombination. One such spectrum of the room temperature photoluminescence from the $Cu_2(I)O$ sample experiencing an off-resonant excitation by a green ($\hbar\omega_{cw} = 2.33\,eV$) cw laser is presented in Figure 3.3.2.

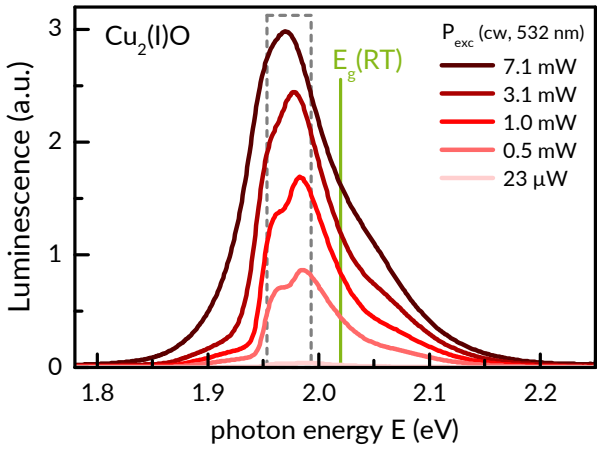

Figure 3.3.2: Room-temperature photoluminescence measurement from the Cu_2O sample. The spectrum is spectrally centered slightly below 2 eV, but reveals a high-energy tail that extends beyond the theoretically predicted room-temperature direct band gap at 2.02 eV [HEH13] of the material.

As it can be seen, the phonon-assisted luminescence is energetically centered around $E_{lum} = 1.97\,eV$ with a spectral width of $\sim 0.1\,eV$ that increases with excitation power. It is found that the spectrum shifts to slightly lower energies at high excitation intensities due to a local heating of the sample that diminishes the band gap. Using E_{lum} as the reference optical transition energy for an electronic transition between valence and conduction band, we proceed by irradiating a signal light field in form of our infrared probe pulses onto the optically excited sample.

Figure 3.3.3 exemplarily reports our measurement results in Cu_2O using probe pulses centered at a photon energy of 0.88 eV. Panel **a** shows the time-resolved pump-probe signal $\Delta T_p/T_p\,(\hat{=}\,T_N)$ obtained from exciting the sample with 60 fs 1.55 eV Ti:sapphire pulses yielding a carrier density of $n_e = 2.4\times10^{19}cm^{-3}$ within its penetration depth of $z_\beta = 7.4\,\mu m$[2]. All data is normalized to the equilibrium probe transmission level prior to the temporal pulse overlap. During the coincidence of both pulses at $\tau = 0\,ps$, the probe undergoes a pump-induced two-photon absorption up to $T_N = -0.04$ represented by the $\Delta\tau \sim 200\,fs$ long dip in transmission representing the

[2]Since Cu_2O has a bandgap above 2 eV, it here is pumped via two-photon absorption with an absorption coefficient of $\beta(1.55\,eV) = 6.6\,cm/GW$ [SRG14].

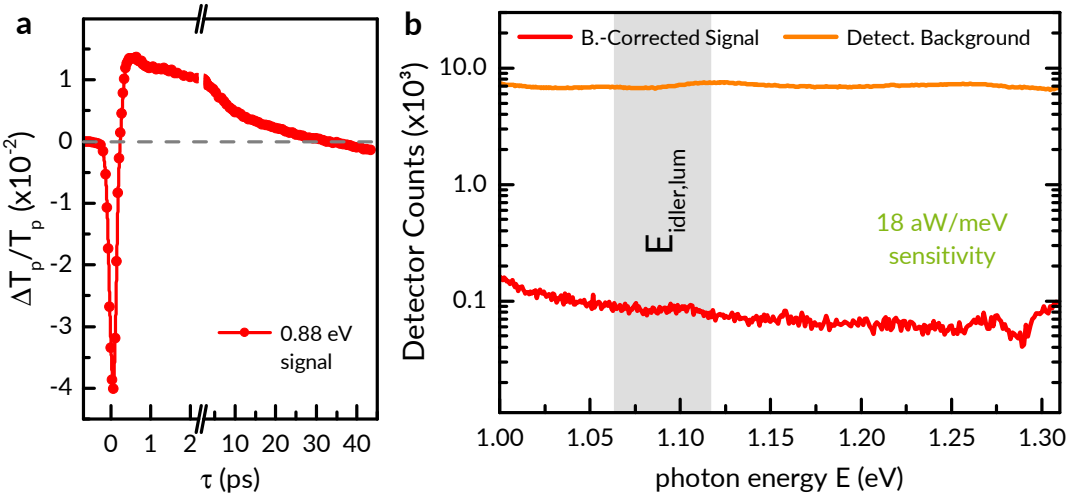

Figure 3.3.3: Transmission measurement data in Cu_2O for a 0.88 eV probe beam. **a**, Pump-probe measurement for a carrier density $n_e = 2.4 \times 10^{19} cm^{-3}$ revealing a $\Delta\tau \simeq 30$ ps gain regime following the optical excitation. **b**, Corresponding spectrum containing the suspected idler emission photon energy interval $E_{idler,lum}$.

pump-probe convolution in the material. In contrast, for elevated pump fluences, here being $I_{exc} = 20.4\,mJ/cm^2$, the relative probe transmission shortly after the pump excitation reveals a signal enhancement of $T_N \simeq 1 \times 10^{-2}$ within a temporal frame of $\tau \sim 30$ ps that may indicate a two-photon gain regime due to the strong carrier injection. Hence it is during this temporal window that we record spectrograms in the subsequent search for idler emission signatures.

As depicted by Figure 3.3.3**b**, we monitor the suspected idler spectral range at a pump-probe delay of $\tau = 3.3$ ps. In order to suppress our spectrally broad fs laser pulses from influencing the sensitive measurement of the potential two-photon emission we use shortpass (1300 nm and 1400 nm) filters in front of the spectrometer for filtering the probe and a 900 nm longpass filter for the pump and parametric amplification remnants in the probe. Furthermore, a spectral background measurement at a pump-probe delay of $\tau = -0.7$ ps (same as the pump-probe measurement reference) is used as a reference spectrum (orange data) for signal subtraction. As previously determined from our luminescence measurements, we expect a central idler photon energy of 1.09 eV for the 0.88 eV signal photons.

However, to our best effort no idler signatures have been detected in our measurements, neither at the predicted idler photon energies (grey box) nor in the adjacent spectral region representing higher sum photon energies further off the band edge. We have applied various excitation densities up to $n_e = 2.2 \times 10^{20}\,cm^{-3}$, but no evidence of

stimulated TPE in this configuration has been found within the sensitivity of our experiment. From spectral measurements of our infrared probe pulses, we determine our detection sensitivity to be at least $\approx 20\,\mathrm{aW/meV}$ which is five orders of magnitude more sensitive then the detected peak idler intensities $P_{idl} \geq 10\,\mathrm{pW/meV}$ reported in [HGO08]. In order to verify the published stimulated idler emission observation in GaAs we have turned to investigate our GaAs samples both with cw and pulsed excitation at similar signal photon energies to *Hayat et al.* A comprehensive list of the employed measurement configurations for GaAs is found in Table 3.1.

sample	excitation laser	$\hbar\omega_{sig}$(eV)
GaAs (100) 800 nm	pulsed, 1.55 eV $n_e \leq 1.5\times10^{19}\,\mathrm{cm^{-3}}$	0.80
		0.71
GaAs (111) 0.5 mm	pulsed, 1.55 eV $n_e \leq 1.8\times10^{19}\,\mathrm{cm^{-3}}$	0.85
		0.83
		0.69
		0.62
	cw, 2.33 eV $n_e \leq 6.0\times10^{17}\,\mathrm{cm^{-3}}$	0.85
		0.78

Table 3.1: Measurement parameters used for the search of stimulated idler emission signatures in room-temperature GaAs. Several signal photon energy tunings to nondegenerate two-photon transitions have been investigated in both pulsed and continuous wave (cw) optically excited samples.

Nevertheless, even for conditions closely resembling the reported experiment, i.e. using a 0.5 mm GaAs(100) sample pumped above the optical bandgap by a green cw laser, we have not detected spectral two-photon idler signatures to the, in this case, 0.85 eV signal pulses irregardless of the excitation intensity.

These findings suggest that rather than stimulated TPE, another mechanism produces the weak signal gain shortly after optical excitation in our pump-probe measurements in Figure 3.3.3**a**. Potentially, the contribution of the electron-hole gas to the dielectric function $\epsilon_r(\omega)$ and therefore the refractive index of the material leads to a defocussing of the probe beam weakening its nonlinear absorption, as well as a slightly diminished reflectivity of the sample facet, especially at high excitation densities. Regarding the nonlinear process itself, the pump-induced population inversion may be incomplete for the addressed two-photon transitions. Therefore, the pump contribution to the sample's nonlinear absorption is directly quantified in the following section.

3.4 Two-photon transparency in GaAs

In the following experiments, we aim to determine the influence of an optical excitation on the nonlinear absorption in GaAs by examining the dependence of pump-induced transmission changes on the probe intensity. In order to provide a homogeneous optical excitation across the sample we begin by investigating the 800 nm thin GaAs layer. Since the IR pulses in our experiment possess photon energies above half the bandgap energy of GaAs at $^1/_2\,E_g = 0.72\,eV$, the probe photons directly address two-photon transitions in the material, besides the so far elusive nondegenerate stimulated idler emission. This stands in contrast to the experiments in Cu_2O and does facilitate an analysis of the excitation-contributed effect since any nonlinear gain in the probe amplitude can be related to an established two-photon inversion rather than relying on a stimulated idler emission process.

During a systematic study of the pump-probe signals at the various probe photon energies available for our experiments, as presented in Figure 3.4.1, we encounter an unexpected behaviour of the signal amplitude. Looking at the probe transmission signal shortly after the pump excitation in Figure 3.4.1**a**, we observe a spectral oscillation of the relative signal amplitude $\Delta T_p/T_p$ on the order of 3×10^{-3} when we apply a comparatively strong optical excitation, in the presented case yielding a carrier density $n_e = 1.3\times10^{19}\,cm^{-3}$. This phenomenon originates from thin film interferences of the probe beam within the sample, also known as Fabry-Pérot or etalon interference. These affect the probe light transmission due to the low near-infrared optical extinction $^I/_{I_0} = e^{-\alpha d} \approx 0.96$ (for $\alpha_{0.9\,eV} = 480\,cm^{-1}$[RM96]) of the sub-micron thick sample that allows for multiple internal probe beam reflections of non-vanishing intensity. The sample then represents an optical resonator where most transmitted spectral modes are suppressed by destructive interference between the phase-shifted reflected partial waves while resonant modes experience an enhanced transmission due to constructive interference. As a result, the etalon transmittance function T, neglecting optical losses, is given by the Airy function [Cra85]

$$T = \frac{1}{1 + F\sin^2(\delta)}, \text{ where } F = \frac{4R}{(1-R)^2}. \tag{3.1}$$

Here, R denotes the surface reflectivity of the sample which is related to the refractive index of the material which has a value of $n_0 \simeq 3.4$ [RM96] at the optical wavelength provided by the probe. Within our experiment, according to the Drude model [Smi59], the intraband free-carrier absorption of both electrons and holes contribute to the dielectric function of the material in direct proportionality to the carrier concentration n_e. The resultant change in refractive index Δn then reads [HLB81]

$$\Delta n = -\left(\frac{e^2\lambda^2}{8\pi^2c^2\epsilon_0 n_0}\right)\left(\frac{1}{m_e}+\frac{1}{m_h}\right)n_e = -0.061 \tag{3.2}$$

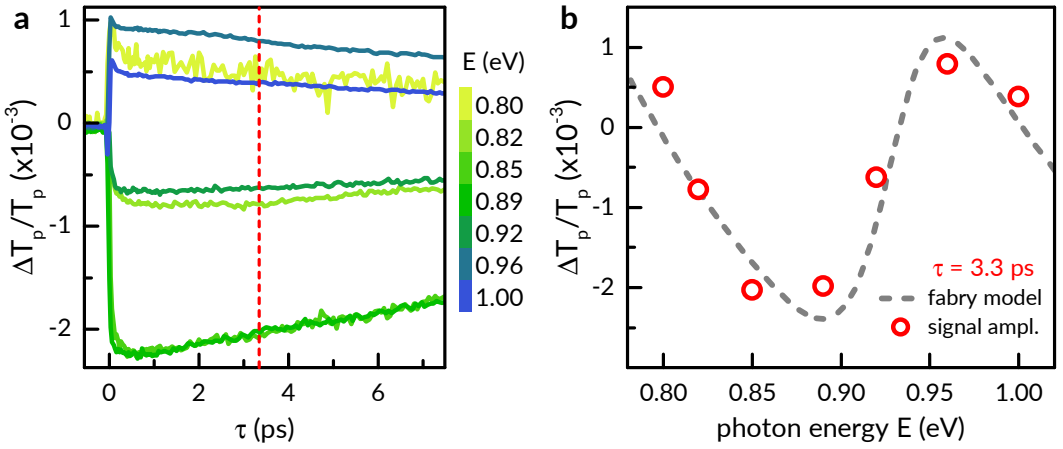

Figure 3.4.1: Pump-probe measurements with $n_e = 1.3 \times 10^{19}\,\mathrm{cm}^{-3}$ at various near-infrared probe photon energies in 800 nm GaAs. **a** The overall pump-probe signal is comparatively weak on the order of $\sim 10^{-3}$, but reveals a periodic amplitude dependence on the probe photon energy. **b** The spectral oscillation of the signal amplitude (evaluated at $\tau = 3.34$ ps) is qualitatively modeled by a phase shift in the sample's Fabry-Pérot interference.

for parameter values relevant to the experiment, i.e. $\lambda_p = 1.4 \times 10^{-6}$ m, $n_0(\lambda_p) = 3.37$ and $n_e = 1.3 \times 10^{19}\,\mathrm{cm}^{-3}$, while using the effective electron and hole masses $m_e = 0.066\,m_0$ and $m_h = 0.3396\,m_0$ for GaAs [Mad04]. Most importantly, the etalon phase δ is specifically sensitive to this refractive index variation Δn, what is expressed by an intensity dependent term added to the initial etalon phase δ_0 given by

$$\delta = \frac{2\pi n d}{\lambda} = \delta_0 + \frac{2\pi \Delta n d}{\lambda}. \tag{3.3}$$

By measuring the pump-probe signal $\Delta T_p/T_p$ we resolve the apparent shift in the etalon phase δ of the transmission function eq. 3.1 by means of the oscillatory signal amplitude offset between the excited and steady state. Indeed, this signal oscillation is well described, cf. Figure 3.4.1**b**, by a model function

$$\frac{\Delta T_p}{T_p} = C_1 \frac{T - T_0}{T_0} + C_2 \tag{3.4}$$

where the fit parameter C_1 considers the optical attenuation of the Fabry-Pérot interference and C_2 references the actual excitation induced signal offset due to free carrier absorption and potential nonlinear gain. As a result, we find that the near-infrared optical response to the pump excitation in 800 nm GaAs is dominated by the appearance of Fabry-Pérot oscillations that exceed the dynamic amplitude of the pump-probe signal. As part of the spectral oscillation, a periodic sign change in

the probe transmission signal is produced that could be misinterpreted as stemming from a stimulated two-photon emission process. Since this interference phenomenon is sensitive to small changes in the refractive index caused by pump-induced charge carriers, it complicates any excitation density dependent studies and may obscure the two-photon related absorption and emission processes.

Hence, for the purpose of isolating an excitation induced modification of the two-photon absorptivity we perform power dependent probe transmission measurements in another GaAs(111) sample with 500 µm thickness. Here our goal is to quantify the variation of the nonlinear absorption coefficient $\Delta\beta$ for a set of increasing excitation intensities. By doing so, an indication of a *two-photon transparency* regime should be obtained, where the optical gain from stimulated two-photon emission events compensates the two-photon absorption losses what effectively leads to $\beta_{\omega_p} + \Delta\beta_{\omega_p} = 0$ at a given probe energy $E_p = \hbar\omega_p$.

In principle, the pump-probe signal ΔT_p can be normalized to the steady state probe transmission T_p which undergoes two-photon absorption. The detected signal is then defined by the changes in absorptivity contributed by the pump excitation, cf. Equation 2.20,

$$\frac{\Delta T_p}{T_p} \approx \Delta\alpha\, z_\alpha + \Delta\beta\, z_\alpha I_p \tag{3.5}$$

within the excitation volume inferred from the pump penetration length $z_\alpha = \alpha^{-1}_{1.55\,eV} = 0.74\,\mu m$ [Asp86]. Due to the intensity scaling of two-photon absorption, eq. 3.5 is approximated by a linear function dependent on the probe intensity I_p which is offset by a carrier induced linear absorption $\Delta\alpha$. Therefore $\Delta\beta$ can be obtained from the slope of the normalized probe transmission signal upon sweeping the irradiated probe intensity I_p.

The result of such a measurement is presented in Figure 3.4.2. The experimental parameters here are chosen similar to the experiment performed in [HGO08]: At room temperature, a $d \sim 100\,\mu m$ GaAs bulk crystal is excited optically above the direct bandgap of the material. Thereby charge carrier densities on the order of $n_e \sim 10^{18}\,cm^{-3}$ are induced within a sub-micrometer volume at the sample facet. In a Lock-In detection scheme, the two-photon absorption of a $E_p = 0.83\,eV$ probe beam referenced to the pump is then monitored in transmission through the sample. In addition, the pump-probe geometry in our case is chosen in a way that the pump beam irradiates the rear facet of the sample so that the full amplitude of the pump-induced two-photon modification can be obtained, because probe photons potentially gained in a stimulated emission process are unlikely to be reabsorbed in the macroscopic sample.

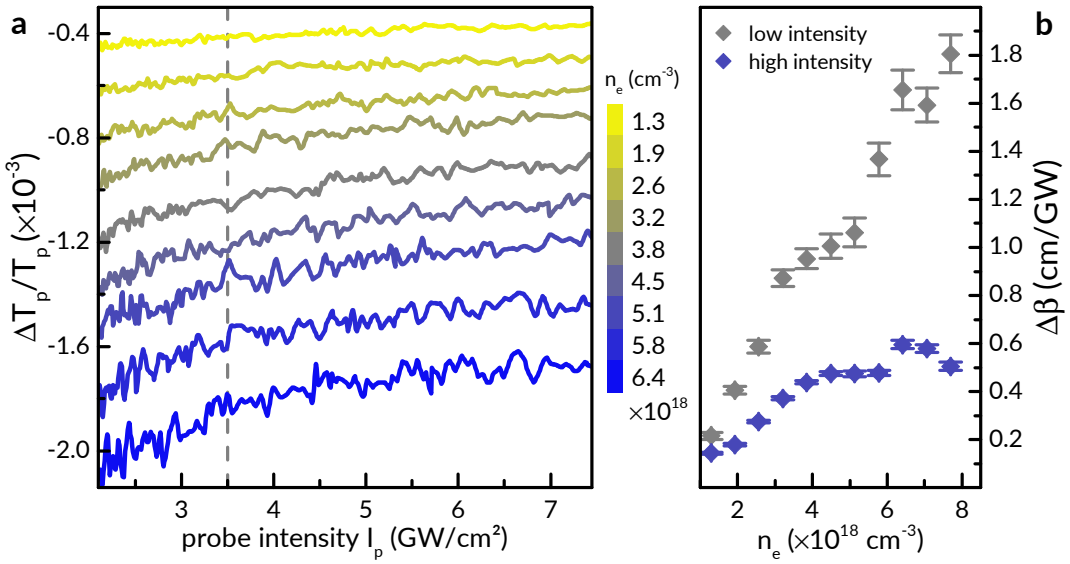

Figure 3.4.2: a Pump-Probe amplitude measurements of the normalized probe transmission in a 500 µm GaAs(111) bulk crystal in dependence of the probe intensity I_p for a photon energy of $E_p = 0.83\,\text{eV}$. Excitation-induced modifications of the two-photon absorption appear as a linear trend. **b** Obtained shift in the two-photon coefficient $\Delta\beta$ over a range of carrier densities in the $n_e \sim 10^{18}\text{cm}^{-3}$ range.

Figure 3.4.2a presents the recorded normalized pump-probe amplitude shortly ($\tau = 3.3\,\text{ps}$) after the pulse overlap for carrier densities n_e ranging from 1.3 to $6.4 \times 10^{18}\,\text{cm}^{-3}$. The overall pump-induced signals are comparatively small on the order of $\Delta T_p/T_p \propto 10^{-3}$, owed to the limited excitation volume. Effectively, a dominant attenuation which increases linearly with the carrier density n_e is found that can be attributed to the enhanced free-carrier absorption in $\Delta\alpha$. Nevertheless, a positive trend in the probe transmission upon increasing the probe fluence I_p is observed across all measurements. As outlined in eq. (3.5), the corresponding $\Delta\beta$ is extracted from a linear fit to the measurement data and plotted in fig. 3.4.2b. At increased densities n_e, we notice a more rapid enhancement of the signal at low I_p compared to higher probe fluences $I_p > 3.5\,\text{GW/cm}^2$ that perturbs the otherwise linear trends. Therefore this regime is treated separately from the high intensity fits which possess a reliable linearity and serves as an upper bound to the shift in the two-photon coefficient $\Delta\beta$.

For the elevated probe intensity regime we find that as a result of the optical excitation the TPA in the excited sample volume appears to be successively weakened by $\Delta\beta = 0.1 - 0.6\,\text{cm/GW}$ for carrier densities up to $n_e = 7.7 \times 10^{18}\,\text{cm}^{-3}$, where it eventually saturates. The upper bound on the two-photon attenuation dictated by

the low intensity slope of $\Delta T_p/T_p$ scales about twice as effective with increased pumping, but does not exceed a value of $\Delta\beta = 1.8\,\mathrm{cm/GW}$ at the highest applied carrier density.

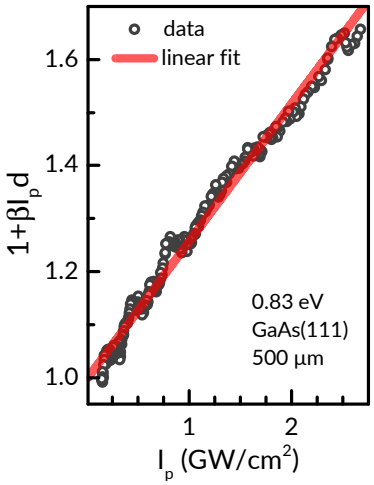

Figure 3.4.3: Fitted two-photon absorption data for a probe photon energy $\hbar\omega_p = 0.83\,\mathrm{eV}$ in GaAs(111).

To set this value into perspective, we have determined the native two-photon coefficient of our GaAs(111) sample to amount to $\beta(0.83\,\mathrm{eV}) = 5.18 \pm 0.04\,\mathrm{cm/GW}$. This value is extracted from a linear fit to inverse probe beam transmissivity $(I_{p,t}/I_p)^{-1} = 1+\beta I_p d$ at $\hbar\omega_p = 0.83\,\mathrm{eV}$ following a two-photon absorption law in dependence of the probe intensity I_p, as depicted in Figure 3.4.3. In conclusion, we find that in the present experimental configuration, the excitation-induced reduction in the two-photon coefficient is about an order of magnitude below the steady-state two-photon coupling coefficient and therefore proves insufficient to achieve *two-photon transparency* or to enter a stimulated TPE regime.

More importantly, the potential signal gain produced by the modified two-photon absorption is greatly outperformed by the competing enhanced linear absorption so that the pump excitation always yields a net absorption, as demonstrated by the escalating negative pump-probe amplitude offset in Figure 3.4.2**a**.

In the light of these findings, the observation of stimulated two-photon emission from ultrafast probe pulses situated at $\hbar\omega_p \geq 0.8\,\mathrm{eV}$ in a bulk GaAs crystal upon injecting a charge carrier density of $n_e \sim 10^{18}\,\mathrm{cm^{-3}}$ via linear optical pumping, as claimed by *Hayat et al.* in [HGO08], does not appear to be feasible. Although an indication for a potential sign reversal of the two-photon coefficient at higher carrier densities $n_e \sim 10^{19} - 10^{20}\,\mathrm{cm^{-3}}$ can be inferred from the upper bounds fit of $\Delta\beta$ in fig. 3.4.2**b**, the emergence of a TPE regime remains questionable due to the observed saturation in the high probe intensity fits, most likely related to the exceeding optical pumping necessary to establish an electronic population inversion sufficiently far off the band edge and across a relevant sample volume. In addition, the pump-induced electron-hole plasma, especially at high densities, modifies the linear optical properties of the sample which may obscure the $\chi^{(3)}$ response. Thus to unambiguously study the dynamic two-photon process under excitation, we implement a more sophisticated measurement technique in the next chapter. On a side note, despite the impactful observations by [HGO08] we are unaware of any studies directly confirming a stimulated idler emission under the presented experimental conditions.

Part IV

Three-beam degenerate pump-probe experiments in CdSe

4 Experimental Methods

In the following, an advanced technique for the study of two-photon interaction in transmission through a semiconductor sample is being presented. The basic measurement principle and scientific foundation of the involved processes are discussed in Section 4.1, while the utilized optical setup is detailed in Section 4.2.

4.1 Time resolved two-photon experiments

In order to gain further insight into the two-photon process under optical excitation, this section introduces a three-beam measurement principle similar to an autocorrelation measurement to be utilized in the following experiments. Such an experimental configuration allows for a temporal resolution of the two-photon interaction and thus makes it possible to study this complex process with more detail. A schematic representation of the principle is illustrated in Figure 4.1.1. In essence, within this scheme two separate laser pulses, the pump and probe, are aligned to impinge onto the sample at a small, but variable temporal delay τ. Only in combination both pulses then address the two-photon transition of an electronic state within the bandstructure of the semiconductor, optionally after a third optical excitation pulse. Such a measurement configuration has been demonstrated to successfully resolve two-photon absorption processes by *Reichert et al.* [Rei16].

In further detail, the probe I_1 is being monitored in transmission under normal incidence onto the sample. It is set to a comparatively weak intensity to avoid any self-induced optical nonlinearities: In the presented experiments the probe-only two-photon absorption is demonstrably small, i.e. $\Delta T_{1,\mathrm{TPA}} \leq 0.05\, T_1$. This circumstance is alleviated by the weak two-photon coupling in vicinity of the band edge (cf. Section 2.4), where the optical control over the absorption can be established. The pump intensity I_2 on the other hand is set to be at least an order of magnitude more intense compared to I_1 in order to trigger the two-photon absorption of probe photons. In that sense, the nonlinear absorption process in propagation direction z in this experiment is described by the coupled differential equations

$$\partial_z I_1 = -\alpha\, I_1 - \beta_{11} I_1^2 - 2\,\beta_{12} I_1 I_2 \simeq -\alpha\, I_1 - 2\,\beta_{12} I_1 I_2 \tag{4.1}$$

$$\partial_z I_2 = -\alpha\, I_2 - \beta_{22} I_2^2 - 2\,\beta_{12} I_1 I_2 \simeq -\alpha\, I_2 - \beta_{22} I_2^2. \tag{4.2}$$

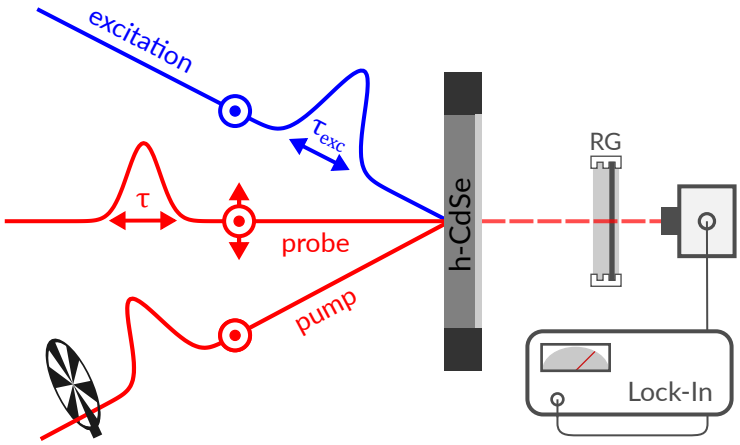

Figure 4.1.1: Schematic representation of the measurement principle. The transmission of the probe pulses (red) through a h-CdSe sample is monitored with an alternable linear polarization and variable pulse time delay. The energetically degenerate pump beam (red, bottom) incides at a small angle to the probe in s-polarization. An optical excitation beam (blue) is optionally being irradiated at an earlier, but also variable time delay to the probe in s-polarization.

These incorporate both linear ($\sim\alpha$) and second order absorption ($\sim\beta$) summands. In the nondegenerate term, the factor of 2 refers to a weak-wave retardation [Van82] which stems from interference between both beams [Wah13] and here ensures that the two-photon coefficient approaches the degenerate case value upon $I_2 \to I_1$. With careful choice of pump and probe intensities during the experiment, the non-dominant absorption terms to the respective beams can be neglected on the right hand side. In effect, the two-photon absorption strength in $I_1(z)$ then is expected to scale linearly with the pump fluence I_2, whereas the pump absorption $I_2(z)$ remains a standard TPA law as introduced in Chapter 2.2. In addition, by the nature of two-photon absorption the individual photons are situated in the spectral transparency region of the material. Therefore, the absorption contributions $\sim\alpha I$ require free charge carrier absorption as a dominant linear process that (safe for intentionally doped samples) has to be achieved by an electronic excitation to the semiconductor. For a description of the mere two-photon correlation transients using only weak fields, these terms also vanish in the limes $\alpha \to 0$, cf. eq. 2.23. As a result, analytical solutions for I(z) here are given by

$$I_1(z) = \frac{I_{1,0}}{(1+\beta(\omega)I_{2,0}z)^2}, \qquad I_2(z) = \frac{I_{2,0}}{1+\beta(\omega)I_{2,0}z}. \tag{4.3}$$

These absorption laws allow for the determination of the two-photon coupling coefficient $\beta(\omega)$ upon measuring the incident and transmitted fluences $I_{1/2,0}$ and $I_1(z)$.

Within the experimental setup, the probe beam is routed across a delay stage to shift it's arrival time τ at the sample facet relative to the pump to allow for temporal resolution. Since the pump beam is periodically modulated, the change in probe transmission due to the pump can be directly obtained via a Lock-In measurement. The recorded signal therefore is a convolution of the Gaussian probe and pump temporal intensity profiles at a fixed delay τ. Such a convolution representing the recorded trace $T(\tau)$ is determined by

$$T(\tau) = [I_1 * I_2](t) = \int I_1(t+\tau) I_2(t)\, dt \tag{4.4}$$

$$= \frac{1}{\sqrt{2\pi}\sigma_1} \frac{1}{\sqrt{2\pi}\sigma_2} \int e^{-\frac{(t+\tau)^2}{2\sigma_1^2}} e^{-\frac{t^2}{2\sigma_2^2}}\, dt$$

$$= \frac{1}{\sqrt{2\pi(\sigma_1^2+\sigma_2^2)}} e^{-\frac{t^2}{2(\sigma_1^2+\sigma_2^2)}}. \tag{4.5}$$

Evidently, the resultant transient $T(\tau)$ is a Gaussian function of τ itself with a temporal width parameter $\sigma_T^2 = \sigma_1^2 + \sigma_2^2$ and reduced amplitude compared to the individual pulses I_1, $I_2(t)$. Since the pump and probe are chosen to be degenerate in the presented experiments, i.e. originating from the same source and therefore identical in pulse duration, one identifies $\sigma_T = \sqrt{2}\,\sigma_1$.

As mentioned before, in addition to the probe and pump pulses addressing the two-photon transition, a third beam may perform an optical excitation of the sample at a variable time delay (usually on the order of picoseconds) prior to the convolution measurements. The effect of this excitation on the two-photon absorption of the probe photons is at the center of this research. In order to suppress any possible contributions to the detected signal due to the Ti:sapphire excitation beam, a RG long pass filter is placed in the path of the typically infrared probe behind the sample. The specifics of the excitation process are covered in more detail in Section 5.1.

One such measurement transient for the two-photon absorption of an ultrashort, near-infrared probe pulse in a 500 µm thick CdSe slab is shown in Figure 4.1.2. Here no prior excitation is applied to the sample so the equilibrium two-photon absorption is observable. As expected, the signal transient in presence of the pump pulse, as seen in panel **a**, has a clearly Gaussian profile with a full width at half maximum $\sigma_{||}^{FWHM} = 68$ fs. In this measurement, the probe and pump are set to a central photon energy $E_\omega = \hbar\omega_p = 0.89$ eV which amounts to a central sum photon energy of 1.78 eV for the two-photon transition. This being only $\simeq 50$ meV above the bandgap energy of the material results in a still comparatively weak two-photon coupling coefficient $\beta_{||} = 0.22$ cm/GW for the co-polarized pump-probe configuration. Nevertheless, the two-photon absorption via the pump pulse yet amounts to a probe absorption factor

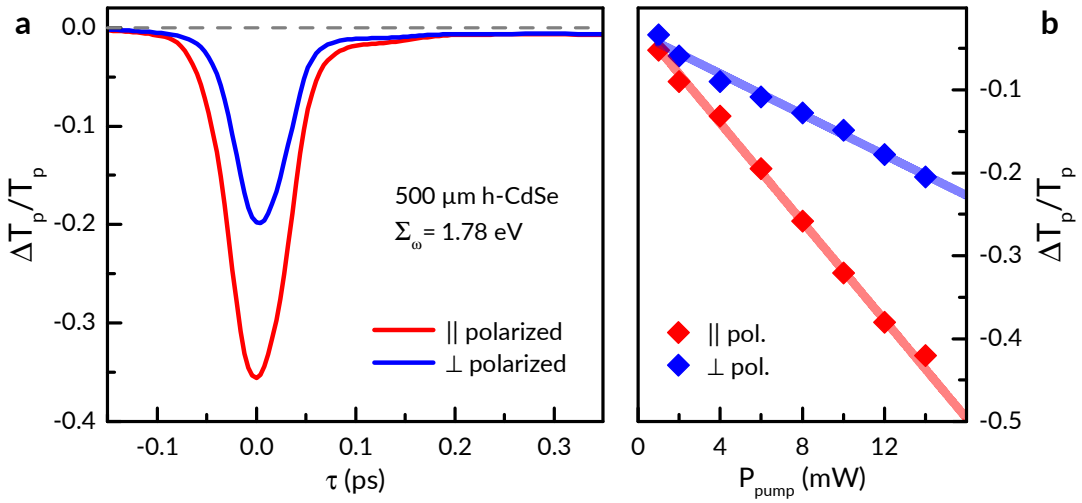

Figure 4.1.2: Time-resolved two-photon absorption measurements in co- (red) and cross-polarized (blue) configuration following the measurement scheme depicted in Figure 4.1.1. A sum photon energy $\sum_{\omega} = 1.78\,\mathrm{eV}$ is investigated in a $500\,\mu\mathrm{m}$ thick h-CdSe sample. **a** During the temporal overlap of both pulses, the co-polarized pump-induced probe pulse absorption amounts up to $\simeq 0.36\,\mathrm{I}_1$. **b** Dependence of the peak two-photon absorption signal on the applied pump power. In both polarization configurations a linear relation consistent with eq. (4.1) is confirmed for the typical pump powers applied in the experiment.

of 0.36 at full temporal overlap $\tau = 0\,\mathrm{ps}$ accross the fairly thick sample. In comparison, setting up pump and probe in a crossed linear polarization yields a notably reduced two-photon absorption amplitude of a factor 0.2 at $\tau = 0\,\mathrm{ps}$ what reveals a more than halfed coupling coefficient $\beta_{\perp} = 0.10\,\mathrm{cm/GW}$. Consequently, a two-photon anisotropy parameter $\beta_{||}/\beta_{\perp} = 0.45$ can be derived at this point, which is well in line with other reports on two-photon experiments in CdSe [Bry74].

The linearity of the TPA strength in $\mathrm{I}_1(z)$ as claimed by Equation 4.1 is confirmed in a seperate measurement as shown in Figure 4.1.2**b**. While using the same optical pump-probe wavelength as before, here the peak signal amplitude $\mathrm{I}_1(\tau = 0)$ is monitored over an order of magnitude in pump power as it is typically applied during the experiment. Both and co- and cross polarized configurations show a reliable linear trend in the absorption amplitude (faint lines). This affirms the suitability of the measurement principle to resolve two-photon absorption in the semiconductor medium.

As an additional observation, one notices a nonvanishing, persistent transmission change $\Delta T \simeq -.03$ at positive delay times τ of the probe relative to the pump. This is owed to the pump undergoing individual two-photon absorption, according to Equation 4.2. The resultant weak optical excitation of electron-hole pairs leads to

free carrier absorption (FCA) of probe photons upon entering the sample. In fact, the exponential thermalization and successive decay $n(\tau) = n_0\, e^{-\tau/\tau_r}$ of these carriers is superposing the two-photon absorption Gaussian for $\tau > 0$ ps what leads to a slight asymmetry in the transient, but can usually be neglected during the data analysis because of its weak influence.

4.2 Experimental setup outline

While the previous section has introduced our experimental approach to time-resolved two-photon interaction, the devised spectroscopic setup is outlined in the following. A schematic illustration of the setup is shown in Figure 4.2.1.

Since the presented experiments employ an all-optical setup, a Ti:sapphire Regenerative Amplifier (RegA) system acts as an ultrafast optical source which generates 1.55 eV modelocked laser radiation. At a repetition rate of 250 kHz the RegA emits 8 µJ low noise pulses of 60 fs duration. That output is split to be used as an optical excitation in the experiment while a larger part of the intensity seeds an Optical Parametric Amplifier (OPA). The OPA generates spectrally tunable near-infrared pulses ($\sim$ 0.75-1 eV) via Difference-Frequency Generation between a white light continuum and the RegA pump. In later experiments, a silicon prism based pulse shaper is subsequently positioned in the OPA beam path to spectrally filter the OPA pulses. This is covered in more detail in Section 5.3.

In any case, the OPA output is split into the energy-degenerate pump and probe beams at a polarizing beam splitter (PBS), where an adjustment of the split power ratio is made possible by means of a half-wave plate ($\lambda/2$). Both the excitation and the probe beam are being routed through retroreflectors mounted to linear motorized stages that enable temporal resolution (≥ 2 fs) following the pump-probe principle discussed in sections 3.2 and 4.1. In addition, Galilei-style telescope arrangements are placed in these optical pathways in order to collimate the laser beams to a diameter w_0 and adjust their focal spot size w_f according to Gaussian optics, i.e. $w_f \sim w_0^{-1}$.

Considering the polarization degree of freedom, both the pump and excitation beams are orientated in linear s-polarization to the sample surface by broadband $\lambda/2$ and polarizer (Glan prism or film polarizer) units that simultaneously allow for a power adjustment of the transmitted pulses. The probe polarization orientation can be rotated via another independent linear polarizer unit, thus allowing for measurement configurations in both co- and cross-polarization between pump and probe.

In order to achieve the necessary power densities ($\sim$GW/cm^2) for two-photon absorption all beams are focused to µm spot sizes. In our experiments, typical probe and

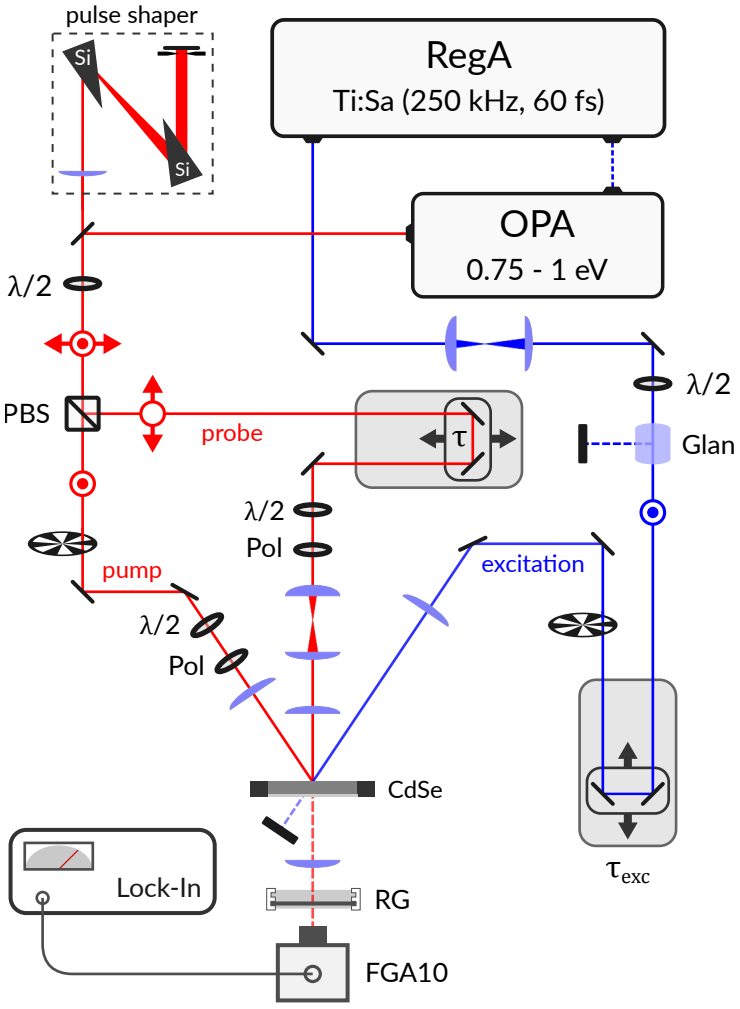

Figure 4.2.1: Outline of the three-beam setup for time-resolved two-photon experiments in CdSe.

pump intensities are $I_{probe} \approx 2\,GW/cm^2$ and $I_{pump} \approx 15\,GW/cm^2$, respectively. As a hierachy, the probe is typically focused down to a spot diameter of 20 µm compared to a pump diameter of 35 µm and excitation spot size of 60 µm. By choosing larger spot sizes, especially for the excitation beam, one intends to spatially homogenize the coinciding laser intensity (having a Gaussian transversal pulse profile) across the probe diameter.

Regarding the three-beam geometry at the sample facet, the probe is aligned perpendicular to the sample while pump and excitation incide at an inclined angle $\theta_i \simeq 20°$, still ensuring a reasonable spatial overlap between all three beams throughout the

sample.

The detection of transient changes in the probe irradiation is achieved by an InGaAs photodiode (FGA10, $\tau_{\text{rise}} = 10\,\text{ns}$) which is placed behind an RG1000 long pass filter that suppresses potential scattered excitation light. All detection is performed in the Lock-In scheme. Here a mechanical chopper periodically modulates ($\simeq 600\,\text{Hz}$) the pump/excitation beam while the probe transmission is being monitored. The Lock-In (SRS SR830) phase-sensitively references the probe signal to the modulation frequency and therefore isolates the transmission variation ΔT related to the respective beam. This makes it possible to detect small signals such as are typical for nonlinear optical processes and, together with the high laser repetition rate, effectively suppresses the signal noise in the measurement data. Therefore, the relative error $\delta x/x$ of an individual datapoint the presented measurements is typically several orders of magnitude below the signal level, i.e. $\delta x/x \simeq 10^{-4}$.

The sample material used in the experiments is a commercial, high resistive (3×10^{11} Ωcm) bulk cadmium selenide crystal in hexagonal configuration (h-CdSe) oriented in <0001> direction. The bulk sample has a thickness $d = 500\,\mu\text{m}$, but $20\,\mu\text{m}$ ground samples are as well used in later measurements. H-CdSe is a direct II-VI semiconductor with a bandgap energy $E_g = 1.73\,\text{eV}$ [Mad04]. The optical two-photon excitation by the RegA pulses ($2\hbar\omega \simeq 3.1\,\text{eV}$) therefore occurs at comparably high transition energies within the CdSe bandstructure while the OPA pump-probe sum energy can be fine-tuned around the bandgap energy.

Regarding its optical properties, CdSe is a long used material in both semiconductor science and technology. In respect to optical nonlinearity, investigations into the two-photon absorption and second harmonic generation properties of bulk CdSe have already been published in the 1970s [Bry74]. Beyond that, while it has seen some use as a photoresistor and as a robust optical medium in infrared Optical Parametric Oscillators [Han74], CdSe is mostly known within the research field of nanoparticles where colloidal CdSe quantum dots show strong, tunable quantum confinement [Maj15]. Here even technological potential for solar cells [Rob06] has been reported. Effectively, CdSe is used as a prototypical direct semiconductor with distinct nonlinear optical properties that at the same time suits our given experimental requirements.

5 Experimental Results

5.1 Saturable Two-Photon Excitation

During the experiments presented in this chapter, the optical excitation of the CdSe sample is performed by the intense $\sim 200\,\mathrm{GW/cm^2}$, 60 fs modelocked pulses from the Ti:sapphire RegA laser source. Having a central photon energy of 1.55 eV, the main absorption mechanism for the excitation pulses is two-photon absorption high above the band-edge of the CdSe semiconductor. To our advantage, this yields a more homogeneous optical excitation profile reaching deeper layers of the sample according to TPA's enhanced penetration depth over linear optical excitation, as stated in Section 2.2. However, one finds that with elevated fluences on the order of $10^{10}\,\mathrm{W/cm^2}$, the occurring two-photon absorption diminishes and reveals a proceeding saturation that limits the achievable carrier densities. There are several mechanisms giving rise to this phenomenon [LGH96]: On the one hand, electric field induced processes including self-phase modulation and Kerr-lensing lead to spectral broadening and potential defocussing which decrease the effective power density in the material. More importantly though, the finite amount of conduction band states reduces the rate at which carriers can be excited whenever the time duration of such intense excitation pulses is shorter than the carrier thermalization time τ_{th} to lower energy states in the band - An expectable circumstance for pulsed laser sources in the fs regime. This is schematically illustrated in Figure 5.1.1**a**. In order to adapt the nonlinear absorption law

$$\mathrm{dI} = -\alpha_2(\mathrm{I})\,\mathrm{I}^2\,\mathrm{dz} \tag{5.1}$$

the nonlinear coefficient α_2 can be modeled as an intensity dependent variable in a hyperbolic approximation according to

$$\alpha_2(\mathrm{I}) = \frac{\alpha_2^0}{1 + \mathrm{I}/\mathrm{I}_{\mathrm{sat}}}. \tag{5.2}$$

The saturation intensity $\mathrm{I}_{\mathrm{sat}}$ here denotes the irradiation required for an effective halving of the absorption parameter α_2 compared to $\alpha_2^0 = \beta(\omega)$. In order to derive these absorption parameters for our experiments, we apply the implicit fit function resulting from the solution to Eq. (5.1) to the reciprocal transmissivity data for a

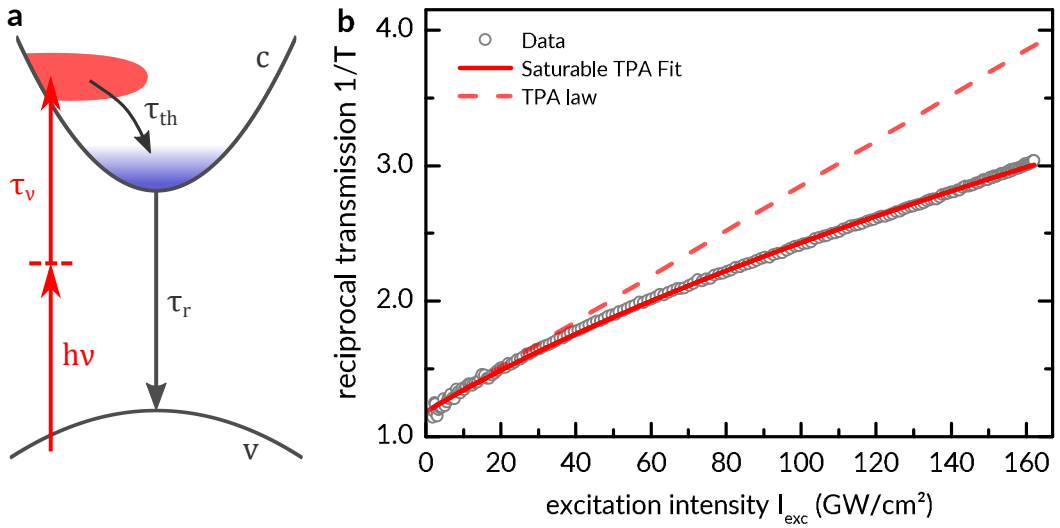

Figure 5.1.1: a Two-photon excitation scheme in a two band model. Carriers are injected at elevated energies into the conduction (c) band within the excitation pulse duration τ_ν and thermalize to the band minimum within τ_{th}. Eventually, the carrier density depletes due to electron-hole recombination within τ_r. **b** Reciprocal transmission data and fit of both the saturable and naive two-photon absorption model for the 1.55 eV excitation Ti:sapphire pulses in a 20 µm h-CdSe sample. A proceeding absorption saturation is observed at high excitation intensities I_{exc}.

variable excitation fluence at the 1.55 eV Ti:sapphire photon energy, as shown in Figure 5.1.1**b**. A front facet reflection coefficient of the sample of $R \simeq 0.26$ has been determined in a seperate reflectivity measurement and is deducted from the input intensity I_{exc}.

As a result, a TPA coefficient $\beta(1.55\,\text{eV}) = 7.0 \pm 0.1\,\text{cm/GW}$ has been extracted from the transmission data of the h-CdSe sample. At elevated excitation intensities $I_0 \geq 50\,\text{GW/cm}^2$ we observe a notable deviation from the standard two-photon absorption law leading to an increased transmission up to a factor of 0.3 at a fluence of $160\,\text{GW/cm}^2$. From our analysis, the characteristic saturation intensity I_{sat} defining the saturable TPA here amounts $I_{sat} = 203 \pm 7\,\text{GW/cm}^2$. Using these parameters in the adapted absorption model allows for a more reliable determination of the charge carrier density n_e within the sample, which one can calculate from the absorbed intensity of the two-photon excitation by

$$n_e\,[\text{cm}^{-3}] = \frac{I_{exc} \cdot (1 - T) \cdot \tau_\nu}{2E_\nu \cdot d}. \tag{5.3}$$

Here d denotes the sample thickness or alternatively the optical (two-photon) penetration depth z_β to yield the respective density parameter while τ_ν characterizes the

optical pulse duration of the laser with photon energy hν. A profound estimation of the carrier density is necessary to reliably determine related parameters such as the conduction band Fermi energy shift ΔE_{F_c}, which is discussed in further detail in Section 5.3.

5.2 Attenuated Two-Photon Absorption

Moving on to the discussion of our experimental results, this section serves as an introduction to the quantitative optical control over the TPA in a bulk semiconductor. In detail, the principle goal of the following experiments is to directly assess the excitation-induced changes to nonlinear absorption in the nondegenerate two-photon configuration. To recapitulate, as outlined in Section 2.4, the absolute value of the bulk semiconductor TPA coefficient $\beta(\omega_{ph})$ depends not only on the second order nonlinear index α_2 at a given photon energy $\hbar\omega_{ph}$, but also on the carrier occupation distributions F_c of the conduction and valence band F_v, i.e.

$$\beta(\omega_{ph}) \propto \alpha_2(\omega_{ph}) \, (F_c(\mathbf{k}) - F_v(\mathbf{k})) \, . \tag{5.4}$$

By optically exciting charge carriers within the sample one increases the occupation probability for electron states in the conduction band. When driven by a resonant light field, these are able to perform stimulated TPE what yields a positive contribution to the, here by definition, negative equilibrium two-photon coefficient that reflects the regular TPA scenario. Eventually, the goal is to achieve a sign change in $\beta(\omega_{ph})$ by establishing an inversion of electron versus hole state occupation throughout the two-photon interaction volume. As for the properties of the light field addressing the two-photon transitions, i.e. the pump and probe beam, the electronic band filling is expected to have the most pronounced impact at transition energies near the band-edge due to the rapid carrier thermalization after excitation, especially in room-temperature experiments. It is therefore that we chose pump-probe spectral tunings just slightly above half the band gap energy of CdSe.

Figures 5.2.1 and 5.2.2 depict the measurements taken at a sum photon energy of $\Sigma_\omega \simeq 1.76\,\mathrm{eV}$ in $500\,\mu\mathrm{m}$ h-CdSe for the case of a strong excitation with $I_{exc} = 13\,\mathrm{mJ/cm^2}$ pulses. Based on the saturable TPA model from Section 5.1, in the process a carrier density $n_e = 6.3{\times}10^{18}\,\mathrm{cm^{-3}}$ is created within an excitation volume with a penetration depth $z_\beta = 16\,\mu\mathrm{m}$ which is clearly identified by the distinct absorption signal in the time-resolved excitation-probe trace for $\Delta T_p/T_p$ shown in Figure 5.2.1.

Here, we observe a decrease in transmission up to $\sim$50% due to the injected charge carrier population. Aside from the temporal overlap of the excitation and probe pulses

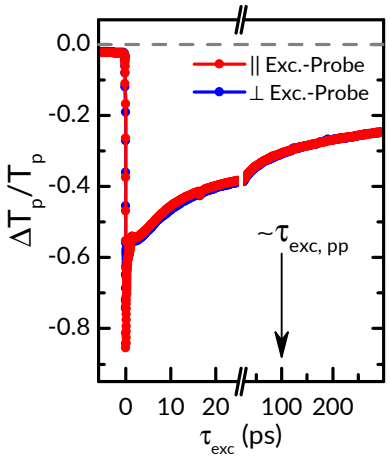

Figure 5.2.1: Excitation-Probe measurements using a strong excitation of $I_{exc} = 13\,mJ/cm^2$.

where nonlinear absorption produces a strong peak signal, the excitation-probe signal is dominated by FCA. It is found that the carrier population rapidly thermalizes within $\sim 10\,ps$ and afterwards produces a steadily declining absorption, where an exponential decay fit to this long-lived signal component indicates a carrier recombination time $\tau_r = 1.34 \pm 0.03\,ns$. Regarding the relative orientation of the linear probe polarization to the excitation beam, it is found that the carrier absorption signal is independent of this degree of freedom. In the following two-photon experiments, we intend to avoid any direct interaction with the excitation pulse and the successive carrier thermalization process and therefore chose to conduct our pump-probe measurements with a nominal delay of $\tau_{exc,pp} \simeq 100\,ps$ to the excitation event.

To visualize the nonlinear response to the sample excitation, Figure 5.2.2**a** reports the probe TPA amplitude in convolution with the pump pulse, i.e. at a fixed pump delay of $\tau = 0\,ps$, with respect to the excitation delay τ_{exc}. Immediately after the excitation, we notice a substantial change of the nonlinear probe transmission owed to an interaction with the excitation pulse itself which dominates the pump signal contribution due its strong intensity with $I_{exc} = 13\,mJ/cm^2$. Because of the different group velocities of the excitation and probe pulses, this direct interaction occurs within a prolonged time window up to $\tau \sim 1\,ps$ before the modified TPA behaviour at the pump-probe photon energy can be extracted. Here, we observe a notable reduction in the peak two-photon amplitude between the unperturbed level at $\tau < 0\,ps$ and post-excitation at $\tau > 2\,ps$ in both co- and cross-polarization configurations. As expected, this TPA offset decreases along with the carrier recombination, but, within the time scope ($\Delta\tau = 250\,ps$) of this measurement, appears to do so at a slower pace than the exponential carrier recombination law applied in Figure 5.2.1, what implies an already very effective occupation of the near-band-edge states involved in the two-photon transitions addressed by the probe.

Upon monitoring the time-resolved (co-polarized) pump-probe convolution shown in Figure 5.2.2**b** at the aforementioned excitation delay $\tau_{exc} = 100\,ps$ we indeed observe a transient bleaching of the TPA, where the pump-induced two-photon amplitude at $\tau = 0\,ps$ (full overlap of both pulses) is reduced by 25%. Since the convolution signal purely arises from the joint TPA of one probe and pump photon, cf. eq. 4.1, this finding is indicative of an excitation-induced reduction of β due to the electronic conduction band population. Considering the TPA magnitude resolved

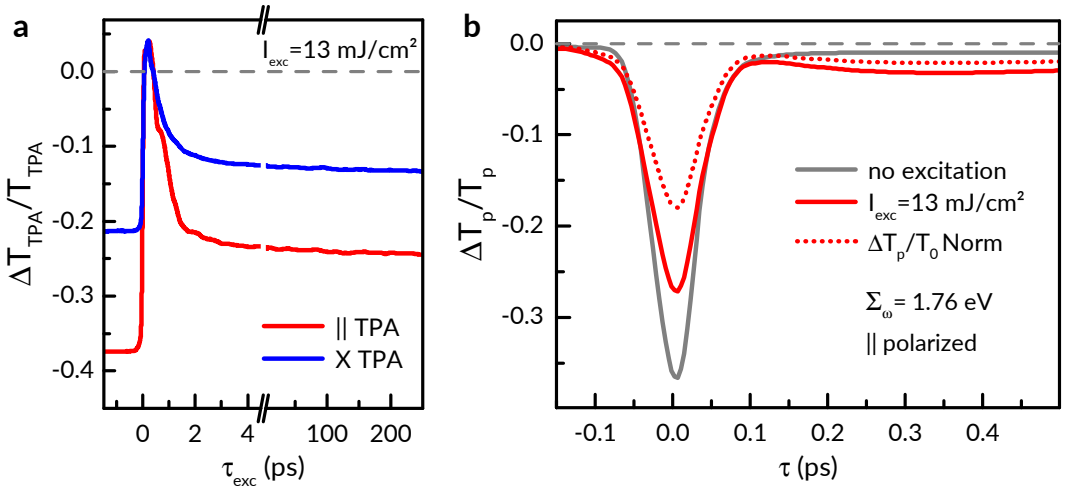

Figure 5.2.2: Probe transmission measurements with $\hbar\omega_p = 0.88\,\mathrm{eV}$. **a** Peak TPA-amplitude T_{TPA} at $\tau = 0\,\mathrm{ps}$ relative to the excitation delay τ_{exc}. **b** Pump-Probe measurements for co-polarized degenerate TPA. A notable attenuation of the nonlinear absorption by $\sim 25\%$ is evident for a delay of $\tau_{exc} = 100\,\mathrm{ps}$ to the sample excitation with $I_{exc} = 13\,\mathrm{mJ/cm^2}$ pulses.

by these measurements, the variation in probe transmission ΔT_p here is normalized to a value in absence of the pump beam T_p, but incorporates the FCA due to the prior excitation. This accurately represents the pump-probe effect determined by the Lock-In technique and therefore the magnitude of the induced TPA, but misrepresents the potential nonlinear gain in reference to the input probe intensity. To that end, the measurement graph scaled to the equilibrium transmission level without excitation T_0 is depicted as the dotted line in panel **b**, which features a mere peak TPA of $\sim 18\%$ of the irradiated probe intensity under the given excitation. As an additional observation, the pump also appears to produce a weakly enhanced probe absorption at longer delays $\tau > 200\,\mathrm{fs}$ after the direct overlap of both pulses. This feature can be attributed to a carrier heating process, where FCA of the pump pulse creates a nonequilibrium carrier distribution which, because of the increased carrier temperature compared to the lattice temperature [Hal90; Wil91; Kri11], in turn enhances the FCA experienced by the probe. Typically, these hot electrons emit their excess energy via electron-phonon scattering within a $\sim$ps relaxation period what results in a limited lifetime of this phenomenon.

In order to quantify the modification of the TPA coefficient $\beta_{exc}(\omega)$ upon optical excitation of the sample, we extract the parameter in an excitation fluence dependent study evaluating the TPA law from Equation 4.3 at the peak signal position during the full pump-probe overlap. Furthermore, to fully exclude the contribution of FCA to the modified probe TPA we utilize measurements of $\Delta T_p/T_p$ in both polarization

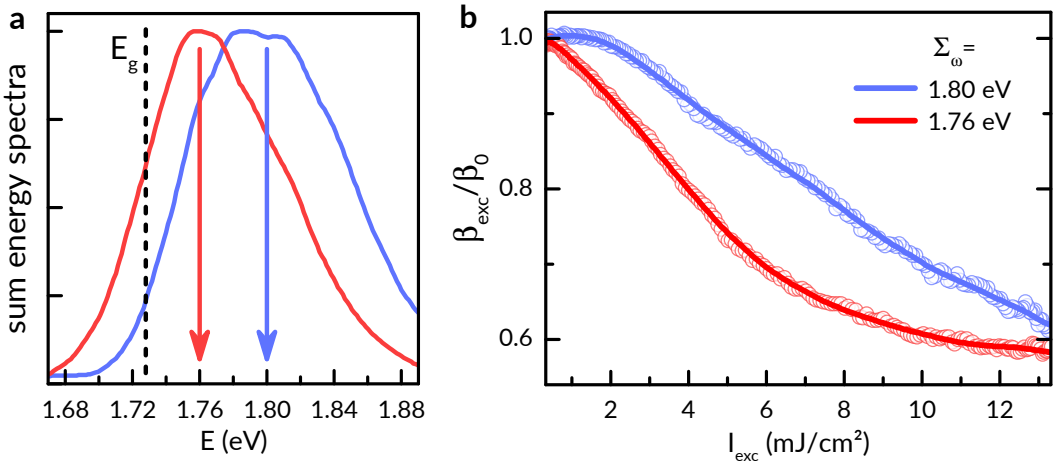

Figure 5.2.3: Excitation-dependent study of the modified two-photon coefficient β_{exc} in 500 µm h-CdSe. **a** Sum energy spectra of two degenerate pump-probe configurations close to the material bandgap E_g. **b** Normalized TPA coefficients 100 ps after optical excitation with up to 13.5 mJ/cm^2 pulses, extracted from the peak pump-probe signal at $\tau = 0$ ps as seen in Figure 5.2.2.

geometries as depicted in Figure 4.1.2. The subtraction of both transients allows for an analysis of the probe intensity I_p according to

$$\left[\frac{\partial I_p}{\partial z}\right]_{\parallel} - \left[\frac{\partial I_p}{\partial z}\right]_{\perp} = -\left(\alpha_{\parallel} - \alpha_{\perp}\right) I_p - \left(\beta_{\parallel} - \beta_{\perp}\right) I_p \cdot I_{pump}. \tag{5.5}$$

Since we attest a fixed relation between $\beta_{\parallel}$ and $\beta_{\perp}$, as outlined by theory sec. 2.3 and the measurement results from fig. 4.1.2**b** and 5.2.2**a**, while the FCA-attributed linear absorption $\sim \alpha_{iso}$ is independent of polarization, as evidenced by the excitation-probe measurements in Figure 5.2.1, the first term vanishes and allows for an extraction of the bare two-photon component from such a measurement.

As shown in Figure 5.2.3**a**, we conduct our analysis for two energetically degenerate pump and probe tunings close to the bandgap at of h-CdSe being $E_g = 1.73$ eV. Besides the aforementioned configuration with a central sum photon energy of $\Sigma_\omega = 1.76$ eV which is directly located at the band-edge, a pump/probe spectrum targeting a slightly higher central sum photon energy of $\Sigma_\omega = 1.80$ eV is investigated, both with an approximate spectral width of $\Delta E_\omega \simeq 100$ meV. Figure 5.2.3**b** illustrates β_{exc} at $\tau_{exc} = 100$ ps normalized to β_0 of the unexcited semiconductor. For both configurations we find a monotonous decrease in the two-photon coupling strength averaged across the entire sample, up to a TPA attenuation of 40% at the highest excitation fluence of $I_{exc} = 13.5$ mJ/cm^2 available in our experiments. More precisely, one observes a more rapid decrease of β_{exc} at $\Sigma_\omega = 1.76$ eV with an apparent saturation from

$I_{exc} = 8\,mJ/cm^2$ onwards than in the case of $\Sigma_\omega = 1.80\,eV$. This finding promotes a rapid filling of near-band-edge states by carrier injection, that produces a Pauli blocking of conduction band states within the excitation volume until the bulk of pump-induced probe TPA in this spectral corridor is exhausted or higher excitation becomes ineffective. In further support of this result, we notice a slightly delayed onset of the TPA attenuation at target sum photon energies higher up in the band with only minimal saturation above $I_{exc} \geq 10\,mJ/cm^2$, but at a similar attenuation value.

To summarize, the present experiments specifically target degenerate TPA near the band-edge of the bulk semiconductor and isolate changes in the TPA strength in response to an intense nonlinear excitation with enhanced penetration depth. In this configuration, our results reveal a substantially stronger attenuation of the (sample-averaged) TPA compared to the singly stimulated experiments in Section 3.4. Nevertheless, no sign change in β indicating a net stimulated two-photon regime has been found, partially owed to saturation effects in the excitable carrier density and limitations of the laser system, but also potentially the damage threshold of the CdSe specimen. Although two-photon gain due to stimulated TPE is not unlikely to occur in the highly excited carrier density layers at the front of the sample, gain-photon re-absorption later in the material here probably always limits the achievable effect on the nonlinear interaction to produce net photon losses. In the following chapter, we intend to further enhance our experimental design by taking a closer look at the relevant parameters towards producing two-photon gain.

5.3 Gain parameters

As introduced in previous chapters, the central figure indicating a spectral regime for two-photon gain characterized by a state occupation inversion is the quasi Fermi energy E_{F_c} associated to the electron concentration n_e in the conduction band. For the near-band-edge electronic states which we investigate in the present experiments, the parabolic band dispersion allows E_{F_c} to be modeled after the 3D Free-Electron Gas [Gru16] with an effective electron mass m_e^*, stating

$$E_{F_c} = \frac{\hbar^2 k_F^2}{2m_e^*} = \frac{\hbar^2}{2m_e^*} \left(3\pi^2 n_e\right)^{2/3}. \tag{5.6}$$

An analogue expression can be used for the valence band occupation level with hole states using their effective mass $m_{d,h}^* = (m_{hh}^{3/2} + m_{lh}^{3/2})^{2/3}$ which at this point can be neglected due to the typically much higher hole mass.

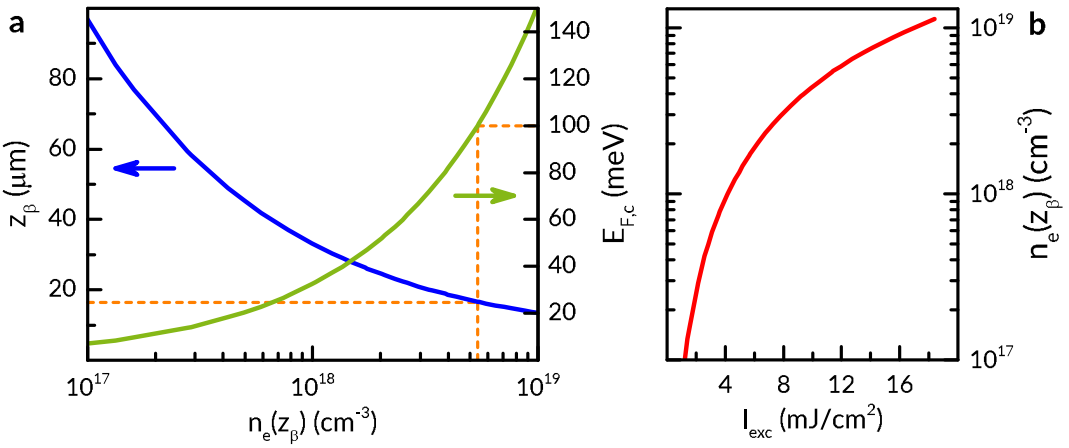

Figure 5.3.1: Excitation-related parameters derived from the saturable absorption model in Section 5.1. The dashed red line references the probe pulse spectral width. **a** Two-photon penetration depth z_β and conduction band quasi Fermi energy E_{F_c} in reference to the carrier density $n_e(z_\beta)$. **b** Excitation intensity I_{exc} and resultant carrier density $n_e(z_\beta)$.

Figure 5.3.1**a** illustrates the resultant quasi Fermi energy E_{F_c} in conjunction with the two-photon excitation depth parameter $z_\beta = (\beta(\omega_{exc})I_{exc})^{-1}$ in our CdSe sample. Both figures are evaluated in dependence of the average carrier density within the excitation volume $n_e(z_\beta)$ which is derived from the saturable TPA model in Section 5.1. In principle, feasible values for E_{F_c} in the range of several 10 meVs for nonlinear gain indeed are obtained at carrier densities above $10^{18}\,\mathrm{cm}^{-3}$, or at excitation pulse intensities $I_{exc} \geq 11\,\mathrm{mJ/cm}^2$, as shown in Figure 5.3.1**b**. Specifically, we find that in order to achieve a sufficient shift in the conduction band Fermi energy in relation to the probe pulse spectral width of $\approx 100\,\mathrm{meV}$ (cf. Figure 5.2.2), a carrier density of $n_e = 5.4 \times 10^{18}\,\mathrm{cm}^{-3}$ is required. At the same time, the excitation laser penetration depth across the displayed $n_e \sim 10^{17} - 10^{19}\,\mathrm{cm}^{-3}$ density regime decreases towards high intensities over a range of $z_\beta \simeq 100 - 20\,\mu\mathrm{m}$, which is notably below the bulk crystal thickness in our experiments - At the critical carrier density, the maximum inversion volume just is established up to a depth of $z_\beta = 17\,\mu\mathrm{m}$ into the sample.

Taking both parameters into consideration, it is evident that a stimulated TPE regime at the semiconductor bandgap relies on high excitation densities approaching $n_e \simeq 10^{19}\,\mathrm{cm}^{-3}$ to produce gain with 60 fs laser pulses. At this high excitation level the inversion is limited to a gain volume within a material depth $d < 20\,\mu\mathrm{m}$. Consequently, it is feasible to chose a sample medium of similar thickness, which we produce by mechanically grinding down a h-CdSe crystal to a thickness of 20 µm for use in further experiments.

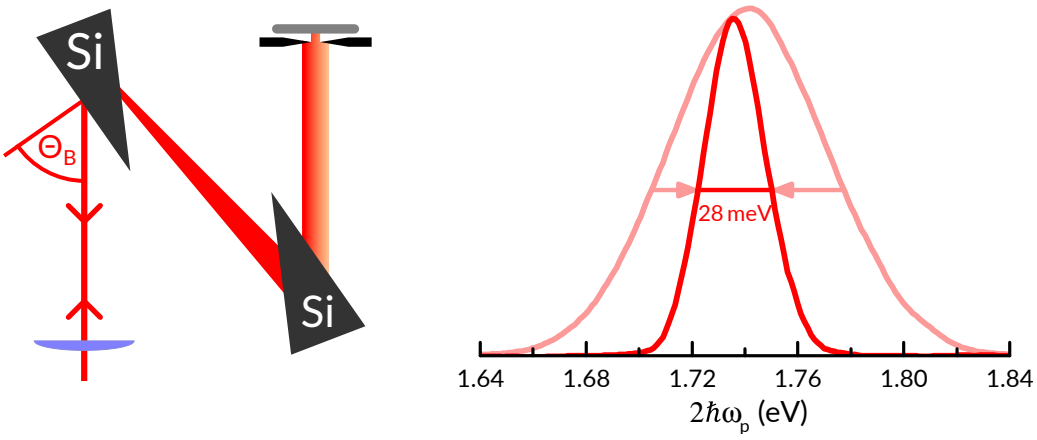

Figure 5.3.2: Si prism-based pulse shaper arrangement used for spectral filtering of the IR beam. A measurement of the (normalized) in- and outcoming pulse spectra demonstrates a significant reduction in bandwidth, typically set to a final value sum photon bandwidth of $\sim$28 meV during the experiment.

In extend, since the use of broadband pulses exacerbates the optical excitation conditions necessary for two-photon gain, we spectrally filter the probe (and pump) pulse by installing a prism-based pulseshaper arrangement, similar to [SYP16], into our experimental setup, where we intend to limit the spectral bandwidth of our fs pulses. As depicted in Figure 5.3.2, this arrangement consists of two wedge-shaped silicon prisms placed inversely orientated to each other along the beam path. At the first prism, our (nearly) circular polarized laser beam is incident under Brewster's angle

$$\Theta_B(\lambda) = \arctan\left(n_{Si}(\lambda)/n_{air}\right) \tag{5.7}$$

in order to reduce optical losses, since the s-polarized light component here is transmitted without reflection. For our optical wavelength being around $\lambda \simeq 1.5\,\mu$m, this results in a steep angle of incidence being $\Theta_B \simeq 74°$. According to Snell's law, Silicon's dispersion of its refractive index $n_{Si}(\lambda)$ in the near infrared produces a wavelength-dependent deflection of the beam components with an angle

$$\Theta_\lambda = \arcsin\left(n_{Si}(\lambda) \cdot \sin(\alpha - \Theta_{Si})\right) \tag{5.8}$$

at the exit facet of the first prism, where α denounces the wedge angle and Θ_{Si} refers to the internal angle of refraction

$$\Theta_{Si} = \arcsin\left(\frac{\sin(\Theta_B)}{n_{Si}(\lambda)}\right). \tag{5.9}$$

within the prism. After passing the second prism at a beam distance |L|, the outgoing light features a lateral split of the laser beam's spectral components with a separation

$$\Delta x = |L| \cdot \left(\tan(\Theta_{\lambda_2}) - \tan(\Theta_{\lambda_1})\right) \tag{5.10}$$

between two wavelength components Θ_{λ_i}. At this point, a movable mechanical slit with adjustable width allows for us to cut out part of the laser spectrum and reduce the spectral bandwidth of the probe (and pump) pulse. For an optimal efficiency a cylindrical lens in front of the arrangement focuses the laser beam into this plane. A subsequent mirror reflects the truncated spectrum along the prism pulse shaper what recombines it into a Gaussian beam.

As illustrated by the spectrograms in Figure 5.3.2, the pulse shaper successfully reduces the spectral bandwidth of the probe pulse, where we achieve a probe bandwidth of $\Delta E = 28\,\text{meV}$ of the (normalized) outgoing 1.74 eV pulse, down from $\Delta E = 71\,\text{meV}$. As a trade off, truncating the pulse spectrum is accompanied by a loss in optical power both due to the partial blocking of light by the slit and an increase in pulse duration as a result of the fundamental time-bandwidth product considering Gaussian pulses

$$\Delta t \Delta \nu \geq 2\ln(2)\,\pi^{-1}. \tag{5.11}$$

This circumstance practically limits the pulse bandwidth during our experiments to provide sufficient optical power for the pump beam to produce a dominant nonlinear optical interaction with the probe.

In effect, the reduction in the pump/probe spectral bandwidth straightforwardly alleviates the carrier density necessary for a two-photon inversion and in consequence enhances the gain volume evoked from the two-photon excitation. In combination with the reduced sample thickness, these measures allow for a more precise study of the near-band-edge excitation effect and potentially overcome the previously found excitation-related limitations towards stimulated two-photon emission.

A third important parameter to be adjusted as part of the experimental design is the probe pulse delay with respect to the excitation pulse which creates the carrier population within the sample. Here a further inspection of the carrier recombination dynamics based on a series of linear excitation-probe measurements with various excitation intensities, see Figure 5.3.3, provides some key insights.

Firstly, it is evident that at any excitation level the carrier thermalization process indicated by the maximum probe attenuation ΔT_p after the excitation-probe overlap occurs within only a few picoseconds ($\tau_{exc} < 5\,\text{ps}$) after the excitation event. This suggests the choice of a similar delay time τ_{exc} close to that value in order to harness

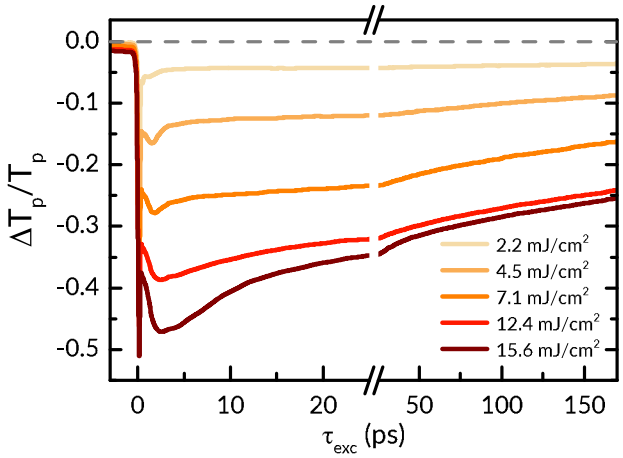

Figure 5.3.3: Excitation-probe measurement series in 20 µm h-CdSe at various excitation intensities up to $I_{exc} = 15.6\,mJ/cm^2$. After an initial thermalization within $\tau_{exc} < 5\,ps$, elevated excitation levels feature a distinctively more rapid short-term carrier recombination.

the maximum available carrier density. In addition, the subsequent decay of the signal recombination reveals a characteristic change in behaviour towards elevated excitation levels: A rapid initial depletion of the carrier population demonstrated by a stronger early decrease in signal amplitude compared to lower excitation intensities is observed. At this point, the high injection densities $n_e > 10^{18}\,cm^{-3}$, cf. Figure 5.3.1, favor a more effective recombination mechanism in form of a dominant Auger process with a shortened carrier lifetime $\tau_A \sim n_e^2$ and the potential contribution of stimulated band-to-band deexcitation. Upon choosing a long excitation-probe delay, this effectively bars our two-photon experiments from accessing a high carrier density regime which consequently emphasizes the usage of shorter pulse delays $\tau_{exc} \sim 10\,ps$.

To summarize, after quantifying the quasi Fermi energy shift E_{F_c} as a result of the optical sample excitation in a model calculation, we have taken measures to establish more favorable experimental conditions towards a net two-photon inversion regime for investigation with near band-edge probe pulses. By producing a mere 20 µm thin sample and limiting the bandwidth of our pump and probe pulses we intend to expand the two-photon gain volume in the excited sample, while we ensure highest carrier induction levels by choosing a suitable few-ps excitation probe delay close to the carrier thermalization window during our experiments.

5.4 Stimulated Two-Photon Emission in thin CdSe

Having developed a better understanding of the experimental conditions necessary for observing stimulated two-photon emission in a direct bulk semiconductor and having performed appropriate modifications to the experimental parameters in Section 5.3, we proceed with a further investigation into the time-resolved two-photon response of our CdSe sample. Large sections of the research presented in this chapter have been published in [Mel18].

In the following introductory measurement set, using the 20 µm thick sample, we utilize pump/probe pulses with an average sum photon energy of $2\hbar\omega_p = 1.78\,\mathrm{eV} \pm 20\,\mathrm{meV}$ (being 40 meV above the material bandgap), now at a moderately short delay of $\tau_{exc} = 12\,\mathrm{ps}$ to our excitation pulses of varying intensity. The resultant pump-probe traces for both co- and cross-polarized configurations are illustrated in Figure 5.4.1. As a first observation, the drastically reduced pulse bandwidth achieved by our prism-based spectral filter in turn leads to an increased pulse duration of 160 fs in this case. Subsequently, the reduced optical power per pulse produces a notably weaker nonlinear response signal when compared to previous measurements such as in Figure 5.2.2, now yielding relative changes to the probe transmission $\Delta T_p/T_p$ just on the order of 10^{-2}. On the other hand, our two-photon measurements here exhibit a strongly enhanced response to the carrier excitation as a result of the modified experimental conditions. Most prominently, we observe a strong attenuation of the TPA signal already at moderate band filling levels. Eventually, we find a sign change of the TPA amplitude above a threshold excitation level of $I_{exc} \geq 5\,\mathrm{mJ/cm^2}$ in both relative polarizations. A further increase in excitation strength up to $I_{exc} = 16.6\,\mathrm{mJ/cm^2}$ eventually produces a full inversion of the two-photon signal, judging from the pump-probe correlation peak amplitude around $\tau = 0\,\mathrm{ps}$, cf. Figure 5.4.1a. This finding indicates the successful creation of a stimulated two-photon emission regime in a bulk semiconductor using a degenerate pump-probe scheme.

As another central observation, the recorded data reveals distinct excitation-related signal contributions to the pump-probe signal beyond the direct pulse overlap window. As previously discussed in Section 5.2, these can be identified as modified FCA signatures due to the interaction of the pump pulse with the carrier population. These are considered to be polarization independent linear optical signatures, which at this point is being further encouraged due to the evident match of the dynamics and quantitative strength of these features when comparing both measurement sets. Furthermore, it may well be assumed that these free-carrier contributions superpose the nonlinear two-photon process we are looking to investigate. Therefore, our studies on the modification of the two-photon transition strength upon optical excitation

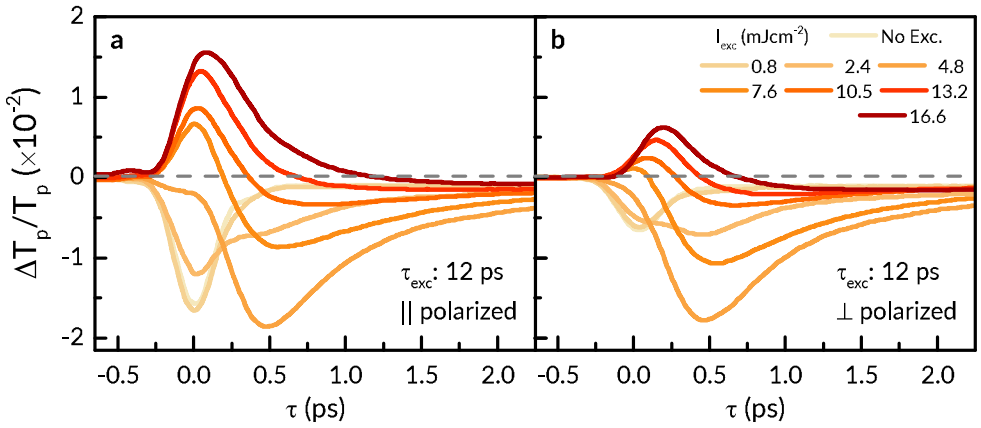

Figure 5.4.1: Two-photon pump-probe measurement set with an average $2\hbar\omega_p = 1.78\,\text{eV} \pm 20\,\text{meV}$ under optical excitation. Both co- (**a**) and cross-linear polarized (**b**) configurations exhibit an enhanced response to the carrier band filling and feature a flip of the transient amplitude sign beyond a threshold excitation with $I_{exc} \approx 5\,\text{mJ/cm}^2$ indicating a TPE regime.

rely on the analysis of the subtracted signal between both relative pump-probe polarization configurations, as detailed by Equation 5.5.

We now demonstrate this method for accessing a two-photon gain signal in a three-pulse scheme in Figure 5.4.2, where we record pump-probe transients with a central sum photon energy $2\hbar\omega_p = 1.80\,\text{eV}$. In the upper panel, both co- ($\parallel$, red) and cross-polarized ($\perp$, blue) pump-probe configurations are shown in direct comparison. Measurements in absence of an optical excitation, here depicted using dashed lines, reflect a steady-state TPA where the co-polarized absorption signal is notably larger by a factor of ~ 2.5 when compared to the cross-polarized TPA case, again as a result of the anisotropy in the third-order optical susceptibility as previously discussed in Section 2.3. For parallel linear-polarized pump and probe beams the overall relative probe attenuation here nets 5%, revealing an absorption coefficient $\beta_\parallel = 1.7\,\text{cm/GW}$. Additionally, after the correlation time window of 230 fs (FWHM) we observe a residual FCA signal with a magnitude of $\sim 1\%$, resulting from a pump-induced carrier excitation. Subsequently, corresponding data in the presence of a preceding strong optical excitation is shown as solid lines in Fig. 5.4.2. Specifically, here we use an excitation-probe delay of $\tau_{exc} = 3.1\,\text{ps}$ and an intensity of $I_{exc} = 16.7\,\text{mJ/cm}^2$, generating a sample averaged carrier density of $n_e = 8.2 \times 10^{18}\,\text{cm}^{-3}$. Similar to the measurement set in Figure 5.4.1, the sign of the differential transmission, in particular during the pump-probe overlap, becomes positive, which indicates an apparent sign reversal of the two-photon coefficient β. Regarding the increase in probe transmission after the pump-probe overlap, this feature again clearly shows to be polarization-independent and arises from a small depletion of the inversion

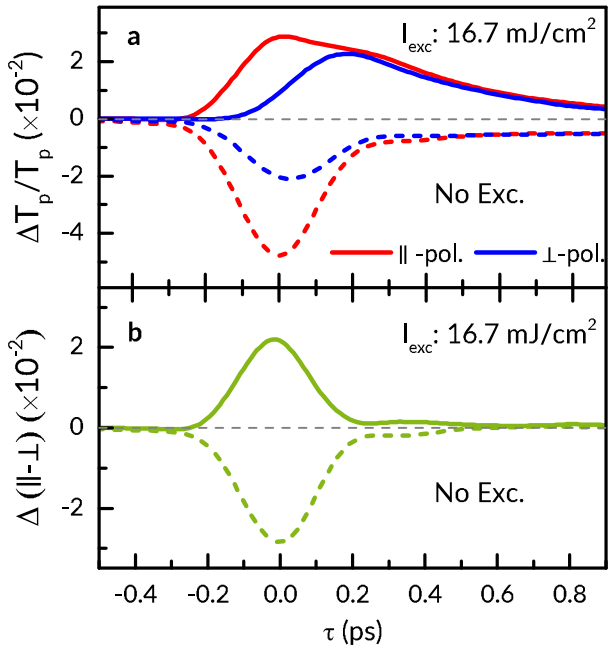

Figure 5.4.2: **a** Pump–probe transients with $2\hbar\omega_p = 1.80\,\mathrm{eV}$ detected with co- ($\parallel$, red) and cross-polarized ($\perp$, blue) configurations. Dashed line, without additional excitation. Solid line, $\tau_{exc} = 3\,\mathrm{ps}$ after optical excitation with a fluence of $I_{exc} = 16.7\,\mathrm{mJ\,/\,cm^2}$. **b** Difference of the pump–probe transients obtained for the two polarization configurations in **a**. While the dashed line refers to the unexcited sample, the solid one represents the case 3 ps after excitation.

by TPA of the pump and a heating-related modification of the FCA. In order to evaluate the nonlinear optical signal, Figure 5.4.2**b** shows the difference of the co- and cross-linear-polarized pump–probe transients presented in Fig. 5.4.2**a** according to $\Delta(\parallel - \perp) = \left([\Delta T_\parallel/T] - ([\Delta T_\perp/T]\right)$ with (solid) and without (dashed) the excitation pulse impinging onto the sample. As expected, this signal subtraction successfully removes transient signals arising from FCAs that can mask the TPE. In contrast, the signal during the pump and probe pulse overlap related to the two-photon transition strength features a complete reversal, which points to the transition from TPA to a similarly strong TPE when population inversion occurs across most of the sample.

Our findings here unambiguously point to two-photon gain in the inversion regime of the optically excited semiconductor. We note, however, that the maximum gain due to TPE is $\sim$3%, i.e., an order of magnitude smaller than the $\sim$40% loss due to FCA seen in the excitation-probe measurements in, for example, Figure 5.3.3 for a similar excitation level. In other words, at this point the comparatively weak two-photon interaction strength in our experiment ultimately prevents us from obtaining a net

optical gain in the probe beam undergoing stimulated TPE within our sample.

In order to further explore the strength of stimulated TPE, we perform measurements for two different pump/probe photon energy tunings closely above half the bandgap energy of h-CdSe with a range of excitation excitation fluences and delay times. As they have been introduced in Figure 5.4.2**a**, we present an exemplary set of differential pump–probe transients $\Delta(\parallel - \perp)$, detected with a moderate excitation-probe delay $\tau_{exc} \simeq 13\,\mathrm{ps}$, in Figure 5.4.4. For these experiments, we apply excitation fluences ranging from zero (yellow line) up to $I_{exc} = 12.3\,\mathrm{mJ/cm^2}$ ($2.0{\cdot}10^{11}\,\mathrm{W/cm^2}$; dark red line). It is our goal to compare the dynamic two-photon transition strength under excitation close to the bandgap energy to a more energetically offset configuration involving states higher in the conduction band. To that end, we irradiate central pump/probe photon energies of 0.885 eV (panel **a**) and 0.90 eV (panel **b**) with their respective pulse spectra shown in Fig. 5.4.3.

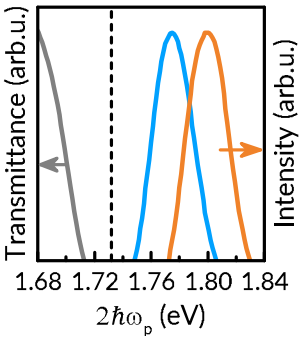

Figure 5.4.3: Pump/probe pulse spectra.

Evaluating our measurements with sum photon energies close to the bandgap investigated in Figure 5.4.4**b**, we observe a full sign reversal of the signal $\Delta(\parallel - \perp)$ when compared to the unexcited semiconductor, similar to our observations in Figure 5.4.2. This finding indicates a full population inversion accross the sample and TPE of similar strength as the steady state TPA in the unexcited semiconductor. Looking at the intermediate excitation levels, we observe a continuously diminished TPA signal from which a threshold power level for an eventual switch between TPA and TPE can be inferred. As a side note, in all of the $\Delta(\parallel - \perp)$ data of this measurement set, a partially dispersive looking deviation from pure Gaussian signals is noticed. This most likely arises from an unintentional chirp of the OPA pulses due to the pulse shaper arrangement introduced to the experiment in Section 5.3. Nevertheless, such a chirp is irrelevant for situations with negligible (very high) excitation, since TPA (TPE) occurs over the entire frequency bandwidth. In contrast, the momentary distribution of pump and probe sum photon energies visibly affects the two-photon transition strength during the pulse overlap for intermediate carrier densities.

Figure 5.4.4**b** shows the corresponding data for an increased pump/probe pulse photon energy of 0.90 eV. As a first observation, the TPA amplitude here increases in comparison to Figure 5.4.4**a**, as illustrated by the yellow line. This is expected from the typical scaling laws for the dispersion of TPA, which display an explicit proportionality to the photon energy $\beta(\omega_p) \propto (2\hbar\omega_p - E_G)^{3/2}$ (in approximation, depending on the band structure model), as detailed in Section 2.3. As before, adding the excitation pulse reduces the magnitude of the TPA. However, the process already

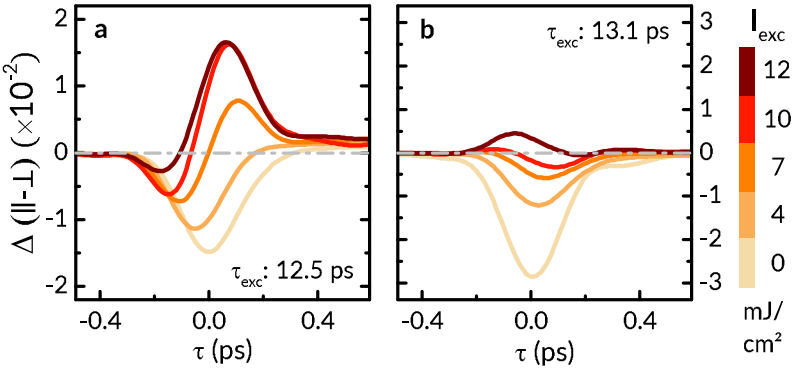

Figure 5.4.4: Differential pump-probe transients $\Delta(\parallel - \perp)$ in the presence of optical excitation for excitation intensities of up to $I_{exc} = 12\,mJ/cm^2$ with a delay time of $\simeq 13\,ps$ after excitation. Data are recorded for central pump/probe photon energies of 0.885 eV (**a**) and 0.90 eV (**b**).

proves to be notably less effective, so that even for the highest excitation level, the observed TPE remains weak, as illustrated by the dark red line in 5.4.4**b**. This result indicates that TPE is most pronounced for pump/probe photon energies very close to $E_G/2$. It is much harder to achieve TPE with increasing excess energy of $2\hbar\omega_p - E_G$. This circumstance can be predicted from the carrier density requirements to achieve a sufficient shift in Fermi energy in the conduction band $\Delta E_{F,c}$ across the sample, as it has been elaborated in Section 5.3. In the present measurements, one finds that an intensity of $12\,mJ/cm^2$ elevates $E_{F,c}$ by an average of 96 meV and provides an effective occupation inversion for the entire probe spectrum centered at 0.885 eV in $\sim$80% of the sample, compared to only $\sim$40% for the 0.90 eV probe spectrum.

In the following, we further explore the requirements for stimulated TPE by taking a closer look at the dependence on excitation fluence I_{exc}, the delay time after excitation τ_{exc}, and the pump/probe photon energy. To that end, we extract $\Delta(\parallel - \perp)$ at the nominal pump-probe overlap $\tau = 0\,ps$ from data sets such as those shown in Figure 5.4.4. and normalize these amplitudes to the value of $-\Delta_0$ of the unexcited CdSe sample. These normalized two-photon amplitudes, dubbed Δ/Δ_0, are displayed im Figure 5.4.5, where values of -1 relate to the TPA in the unexcited semiconductor, while positive values indicate the TPE. Figure 5.4.5**a** illustrates the results for both 0.885 and 0.90 eV pump/probe pulses, i.e. for average sum photon energies $2\hbar\omega_p = 1.77\,eV$ and 1.80 eV, at a delay time of $\tau_{exc} \simeq 13\,ps$. For sum energies of 1.77 eV (red graph), TPA is rapidly bleached when I_{exc} is increased with a pronounced two-photon gain beyond an excitation threshold of $I_{exc} = 6.3\,mJ/cm^2$, followed by an almost full signal inversion that saturates at $10.5\,mJ/cm^2$. In contrast, the measurements at $2\hbar\omega_p = 1.80\,eV$ (blue graph) show a much less pronounced bleaching of the TPA with a notably weaker response to the progressive carrier excitation.

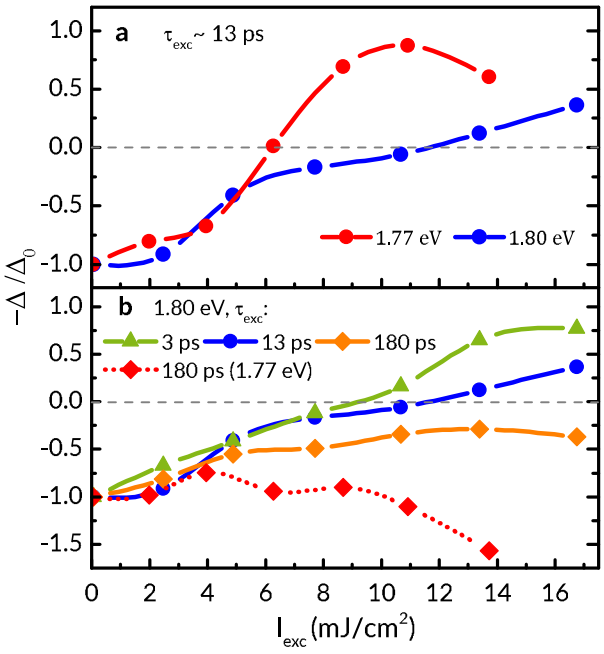

Figure 5.4.5: Amplitudes of the differential pump–probe transients at $\tau = 0$ ps as a function of the excitation fluence I_{exc}. **a** Comparison of the photon energies of $2\hbar\omega_p = 1.77$ eV and 1.80 eV at an excitation delay time of $\tau_{exc} \simeq 13$ ps. **b** Comparison of different time intervals elapsed since photoexcitation, mostly for $2\hbar\omega_p = 1.80$ eV. All data are normalized to the value of Δ_0 seen in the unexcited sample.

Since this configuration addresses higher electron for two-photon transitions, positive two-photon amplitudes Δ/Δ_0 are only found above an elevated threshold excitation with 11.8 mJ/cm^2. Even at the highest excitation fluence $I_{exc} = 16.7$ mJ/cm^2, the transition towards TPE in this case remains incomplete ($-\Delta/\Delta_0 = 0.35$). For this excitation intensity, we estimate a penetration depth of $\sim$10 µm, i.e., thinner than the sample. As a result, stimulated TPE caused by a sufficiently strong population inversion occurs close to the front facet, while TPA still dominates in the rear part. To set these results into perspective, we compare our findings to the previous report on stimulated TPE by *Reichert et al.* [Rei16]. While using a similar three-beam setup, their experiment relies on the use of widely non-degenerate pump and probe photon energies to achieve two-photon gain, as well as an optical excitation via linear absorption. Taking into account the resultant lower penetration depth, their observation of TPE starting at an excitation fluence of 1 mJ/cm^2 is indeed very similar to our findings.

Furthermore, we investigate the dependence of the two-photon transition amplitude on

excitation-probe delay τ_{exc} in Figure 5.4.5**b**. Here we focus on two-photon transitions with a central sum energy of $2\hbar\omega_p = 1.80\,\mathrm{eV}$, since this configuration already displayed more strict conditions for obtaining a stimulated TPE regime. From our data, we find that a just thermalized carrier population at $\tau_{exc} = 3\,\mathrm{ps}$ strongly aides in achieving two-photon gain when compared to $\tau_{exc} = 13\,\mathrm{ps}$, where we obtain TPE above a threshold excitation with $I_{exc} \simeq 9.3\,\mathrm{mJ/cm^2}$ and $I_{exc} \simeq 12\,\mathrm{mJ/cm^2}$, respectively. The rapid initial decay of such high-density carrier populations, as described in Section 5.3, here evidently affects the occupation inversion for two-photon transitions at these elevated band structure states. Therefore, a consciously short excitation-probe delay is favorable towards TPE both in terms of the required optical excitation density and the maximum achievable gain amplitude. Looking at longer excitation-probe delays of $\tau_{exc} = 180\,\mathrm{ps}$ we find that the carrier concentration level is eventually insufficient to maintain an inversion regime at any excitation intensity. As a result, we only see a $\sim 70\%$ attenuation of the TPA. Beyond these findings, we also notice the occurrence of band gap renormalization by lattice heating. Especially by looking at the measurements with of $2\hbar\omega_p = 1.77\,\mathrm{eV}$ (red dotted line), where we again notice the absence of two-photon gain at $\tau_{exc} = 180\,\mathrm{ps}$, we find that, surprisingly, the TPA for elevated fluences is stronger than it is seen in the unexcited sample. For two-photon transitions with this little excess energy, the effect of an intense excitation pulse at such late τ_{exc} can be identified as an enhanced TPA due to bandgap shrinkage as a result of excitation-induced heating: Instead of achieving stimulated TPE events via band occupation with carriers.

In summary, this section has explored the properties of near band-edge TPA and the requirements for obtaining stimulated TPE by tuning the experimental parameters in our three-pulse measurement scheme. As advised by the considerations in Section 5.3, a bandwidth limitation of the irradiated two-photon resonant pulses, as well as limiting the sample volume closer to the excitation penetration depth, strongly aides two-photon gain in our prototypical direct semiconductor. As a result, stimulated TPE from the photoexcited sample has been observed to indeed be as strong as the natural TPA in the unexcited semiconductor. Here, utilizing the full magnitude of the induced carrier population at a short excitation-probe delay $\tau_{exc} \leq 10\,\mathrm{ps}$ and limiting the two-photon excess energy to $2\hbar\omega_p < E_g + 80\,\mathrm{meV}$ have been identified as key strategies. Moreover, lattice heating has been found to impact the two-photon coupling strength via bandgap renormalization which may hinder the observation of TPE. Finally, the threshold excitation pulse intensities for TPE obtained by our investigations emphasize the necessity for an intense optical source, i.e. short-pulsed lasers, to establish a population inversion in a bulk semiconductor by photoexcitation.

6 Conclusions

This thesis has set out to investigate aspects of stimulated two-photon transitions in bulk direct semiconductors with an ultrafast spectroscopy approach. Starting out with an experimental scheme very similar to the initial report on stimulated TPE in GaAs by *Hayat et al.* [HGO08] in Chapter III, the observation of emitted idler photons from a singly stimulated electronic deexcitation has turned out to be surprisingly difficult. It was found that for the applied signal photon detunings far off the optical band edge, the excitation-induced modification of the nonlinear coupling remains far too weak to produce macroscopical TPE, but introduces competing linear optical effects, rendering a replication of the claimed nondegenerate stimulated TPE process at the reported carrier density levels impossible.

Nevertheless, upon a further assessment of the dynamic nonlinear response to optical excitation of h-CdSe in Chapter IV, we have found that the electronic band filling by a strong optical excitation on the order of $I_{exc} \sim 10\,mJ/cm^2$ indeed produces a notable attenuation of the two-photon absorption for target sum photon energies closely above the band gap energy of the sample. Here, the choice of a pulsed two-photon excitation at few ps pulse delay to the investigated probe, whilst subsequently matching the sample thickness to the respective laser penetration depth in the few-μm range, proved instrumental in establishing full optical control over the nonlinear response across the entire medium. As a result, we conclude that rather extreme excitation conditions are necessary in order to ultimately observe stimulated two-photon emission from a bulk semiconductor, where the injected carrier density approaches $n_e \sim 10^{19}\,cm^{-3}$ across said limited gain volume.

Still, in obeying these parameters, we have successfully demonstrated a sign reversal of the nonlinear coefficient $\beta(\omega)$ for a degenerate two-photon scheme that eventually produced a full amplitude inversion in Section 5.4, indicating a two-photon emission regime. From our investigations, it has become evident that the bandwidth of this two-photon gain is dictated by the obtainable shift in Fermi energy $\Delta E_{F,c}$ of the excited semiconductor. In our experiments, we place this corridor within $\Delta E \simeq 80\,meV$ above the optical band gap of the semiconductor. This ultimately places a constraint on the applicable pulse bandwidth for such a two-photon amplification scheme, i.e. for ultrafast pulses with several tens of fs durations.

Furthermore, this work has elaborated on the accompanying effects of the optical excitation on the semiconductor medium. Besides two-photon absorption saturation during the excitation process, discussed in Section 5.1, and indications of band gap renormalization noted in Section 5.4, the contributions to the linear optical refractive index of the material caused by the injected electron-hole plasma have been most prominent. Other than by inducing spectral oscillations in very thin samples, cf. Section 3.4, a pronounced free carrier absorption imposed on the probe beam dominates the transient dynamics. Especially when looking at the stimulated two-photon emission configurations which rely on highly elevated carrier densities, the optical losses due to FCA vastly outperform the achieved nonlinear gain by an order of magnitude. This circumstance effectively suppresses a net two-photon optical gain as a result of the comparatively weak two-photon coupling.

Fortunately, the utilization of widely nondegenerate pump-probe photon schemes, i.e. the pump and probe pulses having notably different photon energies, has the potential of enhancing the two-photon coupling $\beta(\omega_1, \omega_2)$ by several orders of magnitude, as has been shown both theoretically [She91] and experimentally [Cir11], and therefore potentially overcomes the competing linear losses. Here, a careful implementation, possibly in a specifically tailored sample medium, of the required parameters and conditions for stimulated two-photon emission that have been identified in this work into a two-colour pump-probe scheme may point forward towards the full realization of bulk semiconductor-based two-photon gain.

Part V

Appendix

Bibliography

[ACP89] R. Adair, L. L. Chase, and S. A. Payne. "Nonlinear refractive index of optical crystals". *Phys. Rev. B* **39** (1989). DOI: 10.1103/PhysRevB.39.3337.

[Agr89] Govind P. Agrawal. *Nonlinear Fiber Optics*. Academic Press, Inc. (London) Ltd., 1989.

[Asp86] D. E. Aspnes et al. "Optical properties of $Al_xGa_{1-x}As$". *Journal of Applied Physics* 60 (1986). DOI: 10.1063/1.337426.

[Bas62] M. Bass et al. "Optical Rectification". *Phys. Rev. Lett.* **9** (1962). DOI: 10.1103/PhysRevLett.9.446.

[BEL95] S. Bay, M. Elk, and P. Lambropoulos. "Aspects of the degenerate two-photon laser". *Journal of Physics B: Atomic, Molecular and Optical Physics* **28** (1995). DOI: 10.1088/0953-4075/28/24/019.

[Boy08] Robert W. Boyd. *Nonlinear Optics*. Elsevier Science & Technology, 2008.

[Bry74] F. Bryukner et al. "Two-photon absorption in cadmium selenide". *Soviet Journal of Quantum Electronics* **4** (1974).

[CCK66] R. L. Carman, R. Y. Chiao, and P. L. Kelley. "Observation of Degenerate Stimulated Four-Photon Interaction and Four-Wave Parametric Amplification". *Phys. Rev. Lett.* **17** (1966). DOI: 10.1103/PhysRevLett.17.1281.

[Cir11] C. M. Cirloganu et al. "Extremely nondegenerate two-photon absorption in direct-gap semiconductors [Invited]". *Opt. Express* **19** (2011). DOI: 10.1364/OE.19.022951.

[Cla69] J. F. Clauser et al. "Proposed Experiment to Test Local Hidden-Variable Theories". *Phys. Rev. Lett.* **23** (1969). DOI: 10.1103/PhysRevLett.23.880.

[Cra85] D. Craig et al. "Two photon induced optical bistability in CdHgTe at room temperature". *IEEE Journal of Quantum Electronics* **21** (1985). DOI: 10.1109/JQE.1985.1072816.

[DC16] V. Degiorgio and I. Cristiani. *Photonics: A Short Course*. Springer International Publishing, 2016. DOI: 10.1007/978-3-319-20627-1_4.

[Dir27] P. A. M. Dirac. "The quantum theory of dispersion". *The Royal Society* **114**.769 (1927). DOI: 10.1098/rspa.1927.0071.

[Dvo94] M. D. Dvorak et al. "Measurement of the anisotropy of two-photon absorption coefficients in zincblende semiconductors". *IEEE Journal of Quantum Electronics* **30** (1994). DOI: 10.1109/3.283768.

[Fra61] P. A. Franken et al. "Generation of Optical Harmonics". *Phys. Rev. Lett.* **7** (1961). DOI: 10.1103/PhysRevLett.7.118.

[FRW87] D. Fröhlich, K. Reimann, and R. Wille. "Time-Resolved Two-Photon Emission in Cu2O". *Europhysics Letters (EPL)* **3** (1987). DOI: 10.1209/0295-5075/3/7/013.

[Gau92] D. J. Gauthier et al. "Realization of a continuous-wave, two-photon optical laser". *Phys. Rev. Lett.* **68** (1992). DOI: 10.1103/PhysRevLett.68.464.

[Göp31] M. Göppert-Mayer. "Über Elementarakte mit zwei Quantensprüngen". *Annalen der Physik* **401**.3 (1931). DOI: 10.1002/andp.19314010303.

[Gru16] Marius Grundmann. *The Physics of Semiconductors - An Introduction Including Nanophysics and Applications*. 3rd ed. Springer International Publishing, 2016. DOI: 10.1007/978-3-319-23880-7.

[Hal90] K. L. Hall et al. "Femtosecond gain dynamics in InGaAsP optical amplifiers". *Applied Physics Letters* **56** (1990). DOI: 10.1063/1.103085.

[Han74] D. C. Hanna et al. "CdSe down-converter tuned from 9.5 to 24 m". *Applied Physics Letters* **25** (1974). DOI: 10.1063/1.1655414.

[HEH13] M. Heinemann, B. Eifert, and C. Heiliger. "Band structure and phase stability of the copper oxides Cu_2O, CuO, and Cu_4O_3". *Phys. Rev. B* **87** (2013). DOI: 10.1103/PhysRevB.87.115111.

[HFI93] D. R. Heatley, W. J. Firth, and C. N. Ironside. "Ultrashort-pulse generation using two-photon gain". *Opt. Lett.* **18** (1993). DOI: 10.1364/OL.18.000628.

[HGO07] A. Hayat, P. Ginzburg, and M. Orenstein. "High-rate entanglement source via two-photon emission from semiconductor quantum wells". *Phys. Rev. B* **76** (2007). DOI: 10.1103/PhysRevB.76.035339.

[HGO08] A. Hayat, P. Ginzburg, and M. Orenstein. "Observation of two-photon emission from semiconductors". *Nature Photonics* **2** (2008). DOI: 10.1038/nphoton.2008.28.

[HLB81] C. H. Henry, R. A. Logan, and K. A. Bertness. "Spectral dependence of the change in refractive index due to carrier injection in GaAs lasers". *Journal of Applied Physics* **52** (1981). DOI: 10.1063/1.329371.

[HNO09] A. Hayat, A. Nevet, and M. Orenstein. "Electrically Induced Two-Photon Transparency in Semiconductor Quantum Wells". *Phys. Rev. Lett.* **102** (2009). DOI: 10.1103/PhysRevLett.102.183002.

[HS92] D. C. Hutchings and E. W. Van Stryland. "Nondegenerate two-photon absorption in zinc blende semiconductors". *J. Opt. Soc. Am. B* **9** (1992). DOI: 10.1364/JOSAB.9.002065.

[HW94] D. C. Hutchings and B. S. Wherrett. "Theory of anisotropy of two-photon absorption in zinc-blende semiconductors". *Physical review. B, Condensed matter* **49** (1994). DOI: 10.1103/PhysRevB.49.2418.

[Iro92] C. N. Ironside. "Two-photon gain semiconductor amplifier". *IEEE Journal of Quantum Electronics* **28** (1992). DOI: 10.1109/3.135201.

[Ito98] T. Ito et al. "Optical Properties of Cu_2O Studied by Spectroscopic Ellipsometry". *Journal of the Physical Society of Japan* **67** (1998). DOI: 10.1143/JPSJ.67.2125.

[Kan57] E. Kane. "Band structure of indium antimonide". *Journal of Physics and Chemistry of Solids* **1** (1957), pp. 249–261. DOI: 10.1016/0022-3697(57)90013-6.

[Kan80] E. O. Kane. "Band structure of narrow gap semiconductors". *Narrow Gap Semiconductors Physics and Applications*. Ed. by Wlodek Zawadzki. Springer Berlin Heidelberg, 1980, pp. 13–31.

[Kaz14] T. Kazimierczuk et al. "Giant Rydberg excitons in the copper oxide Cu_2O". *Nature* **514** (2014). DOI: 10.1038/nature13832.

[Kel65] L.V. Keldysh. "Ionization in the field of a strong electromagnetic wave". *Sov. Phys. JETP* **20** (1965).

[Kri11] S. Krishnamurthy et al. "Temperature- and wavelength-dependent two-photon and free-carrier absorption in GaAs, InP, GaInAs, and InAsP". *Journal of Applied Physics* **109** (2011). DOI: 10.1063/1.3533775.

[Kro62] N. M. Kroll. "Parametric Amplification in Spatially Extended Media and Application to the Design of Tuneable Oscillators at Optical Frequencies". *Phys. Rev.* **127** (1962). DOI: 10.1103/PhysRev.127.1207.

[Kum04] P. Kumar et al. "Photonic Technologies for Quantum Information Processing". *Quantum Information Processing* **3** (2004). DOI: 10.1007/s11128-004-3102-4.

[Lam67] P. Lambropoulos. "Quantum Statistics of a Two-Photon Quantum Amplifier". *Phys. Rev.* **156** (1967). DOI: 10.1103/PhysRev.156.286.

[LF74] C. C. Lee and H. Y. Fan. "Two-photon absorption with exciton effect for degenerate valence bands". *Phys. Rev. B* **9** (1974). DOI: 10.1103/PhysRevB.9.3502.

[LGH96] J.-F. Lami, P. Gilliot, and C. Hirlimann. "Observation of Interband Two-Photon Absorption Saturation in CdS". *Phys. Rev. Lett.* **77** (1996). DOI: 10.1103/PhysRevLett.77.1632.

[LLM41] G. N. Lewis, D. Lipkin, and T. T. Magel. "Reversible Photochemical Processes in Rigid Media. A Study of the Phosphorescent State". *Journal of the American Chemical Society* **63** (1941). DOI: 10.1021/ja01856a043.

[LNT65] M. Lipeles, R. Novick, and N. Tolk. "Direct Detection of Two-Photon Emission from the Metastable State of Singly Ionized Helium". *Phys. Rev. Lett.* **15** (1965). DOI: 10.1103/PhysRevLett.15.690.

[Mad04] Otfried Madelung. *Semiconductors: Data Handbook*. Springer-Verlag Berlin Heidelberg New York, 2004. DOI: 10.1007/978-3-642-18865-7.

[Mai60] T. H. Maiman. "Stimulated Optical Radiation in Ruby". *Nature* **187** (1960). DOI: 10.1038/187493a0.

[Maj15] A. Majdabadi et al. "Investigation of stability and nonlinear optical properties CdSe colloidal nanocrystals". *Journal of Laser Applications* **27** (2015). DOI: 10.2351/1.4915540.

[Man79] L. Mandel. "Sub-Poissonian photon statistics in resonance fluorescence". *Opt. Lett.* **4** (1979). DOI: 10.1364/OL.4.000205.

[Mel18] S. Melzer et al. "Stimulated two-photon emission in bulk CdSe". *Opt. Lett.* **43** (2018). DOI: 10.1364/OL.43.005066.

[NHO10a] A. Nevet, A. Hayat, and M. Orenstein. "Measurement of Optical Two-Photon Gain in Electrically Pumped AlGaAs at Room Temperature". *Phys. Rev. Lett.* **104** (2010). DOI: 10.1103/PhysRevLett.104.207404.

[NHO10b] A. Nevet, A. Hayat, and M. Orenstein. "Ultrafast pulse compression by semiconductor two-photon gain". *Opt. Lett.* **35** (2010). DOI: 10.1364/OL.35.003877.

[NW67] G. H. C. New and J. F. Ward. "Optical Third-Harmonic Generation in Gases". *Phys. Rev. Lett.* **19** (1967). DOI: 10.1103/PhysRevLett.19.556.

[NZT81] B. Nikolaus, D. Z. Zhang, and P. E. Toschek. "Two-Photon Laser". *Phys. Rev. Lett.* **47** (1981). DOI: 10.1103/PhysRevLett.47.171.

[Ota11] Y. Ota et al. "Spontaneous Two-Photon Emission from a Single Quantum Dot". *Phys. Rev. Lett.* **107** (2011). DOI: 10.1103/PhysRevLett.107.233602.

[Pid79] C. R. Pidgeon et al. "Two-Photon Absorption in Zinc-Blende Semiconductors". *Phys. Rev. Lett.* **42** (1979). DOI: 10.1103/PhysRevLett.42.1785.

[Pid80] C. R. Pidgeon. *Free Carrier Optical Properties of Semiconductors*. Handbook on Semiconductors, Vol. 2. North Holland, Amsterdam, 1980.

[Rei16] M. Reichert et al. "Observation of Nondegenerate Two-Photon Gain in GaAs". *Phys. Rev. Lett.* **117** (2016). DOI: 10.1103/PhysRevLett.117.073602.

[RM96] A. D. Rakić and M.L. Majewski. "Modeling the optical dielectric function of GaAs and AlAs: Extension of Adachi's model". *Journal of Applied Physics* **80** (1996). DOI: 10.1063/1.363586.

[Rob06] I. Robel et al. "Quantum Dot Solar Cells. Harvesting Light Energy with CdSe Nanocrystals Molecularly Linked to Mesoscopic TiO2 Films". *Journal of the American Chemical Society* **128** (2006). DOI: 10.1021/ja056494n.

[SB64] P. P. Sorokin and N. Braslau. "Some Theoretical Aspects of a Proposed Double Quantum Stimulated Emission Device". *IBM Journal of Research and Development* **8** (1964). DOI: 10.1147/rd.82.0177.

[She91] M. Sheik-Bahae et al. "Dispersion of bound electron nonlinear refraction in solids". *IEEE Journal of Quantum Electronics* **27** (1991). DOI: 10.1109/3.89946.

[Smi59] R. A. Smith. *Semiconductors*. 1st ed. Cambridge University Press, 1959.

[SRG14] J. Serna, E. Rueda, and H. García. "Nonlinear optical properties of bulk cuprous oxide using single beam Z-scan at 790 nm". *Applied Physics Letters* **105** (2014). DOI: 10.1063/1.4901734.

[SSS89] M. Sheik-bahae, A. A. Said, and E. W. Van Stryland. "High-sensitivity, single-beam n_2 measurements". *Opt. Lett.* **14** (1989). DOI: 10.1364/OL.14.000955.

[Sto73] R. H. Stolen. "Optical Kerr Effect in Glass Waveguide". *Applied Physics Letters* **8** (1973). DOI: 10.1063/1.1654644.

[Str85] E. W. Van Stryland et al. "Energy band-gap dependence of two-photon absorption". *Opt. Lett.* **10** (1985). DOI: 10.1364/OL.10.000490.

[SYP16] Y. Shaked, S. Yefet, and A. Pe'er. "The Prism-Pair: Simple Dispersion Compensation and Spectral Shaping of Ultrashort Pulses". *Int J Exp Spectroscopic Tech* **1** (2016). DOI: 10.35840/2631-505X/8507.

[Van82] E. Van Stryland et al. "Weak-Wave Retardation and Phase-Conjugate Self-Defousing in Si". *Applied Physics B* **29** (1982). DOI: 10.1007/978-3-642-87864-0_89.

[Wah13] J. K. Wahlstrand et al. “Effect of two-beam coupling in strong-field optical pump-probe experiments”. *Phys. Rev. A* **87** (2013). DOI: 10.1103/PhysRevA.87.053801.

[Wal03] Z. D. Walton et al. “One-way entangled-photon autocompensating quantum cryptography”. *Phys. Rev. A* **67** (2003). DOI: 10.1103/PhysRevA.67.062309.

[Wei81] M. H. Weiler. “Nonparabolicity and exciton effects in two-photon absorption in zincblende semiconductors”. *Solid State Communications* **39** (1981). DOI: 10.1016/0038-1098(81)90042-9.

[Whe84] B. S. Wherrett. “Scaling rules for multiphoton interband absorption in semiconductors”. *J. Opt. Soc. Am. B* **1** (1984). DOI: 10.1364/JOSAB.1.000067.

[Wil91] M. Willatzen et al. “Nonlinear gain suppression in semiconductor lasers due to carrier heating”. *Photonics Technology Letters, IEEE* **3** (1991). DOI: 10.1109/68.87928.

[YRB68] S. Yatsiv, M. Rokni, and S. Barak. “Enhanced Two-Proton Emission”. *Phys. Rev. Lett.* **20** (1968). DOI: 10.1103/PhysRevLett.20.1282.

Publications and Contributions

- EDISON'19, Salamanca, Spain - June 2015
  Contributed poster on "Ultrafast Optical Control over the Exciton-Polariton Propagation in CdZnTe"
- J. Lohrenz, S. Melzer, C. Ruppert, I. A. Akimov, H. Mariette, M. Reichelt, A. Trautmann, T. Meier, and M. Betz
  "Ultrafast dynamical response of the lower exciton-polariton branch in CdZnTe"
  Phys. Rev. B **93**, 075201 - Published 2 February 2016
- SPIE Photonics West, San Francisco, USA - January 2018
  Contributed talk on "Stimulated Two-Photon Emission in CdSe"
- S. Melzer, C. Ruppert, A. D. Bristow, and M. Betz
  "Stimulated two-photon emission in bulk CdSe"
  Opt. Lett. **43**, 5066-5069 - Published 11 October 2018

Supervised theses:

- M.Sc. Manfred Janzen, TU Dortmund, 2015
  "Aspekte von Zwei-Photonen-Prozessen in GaAs und Cu_2O"
- M.Sc. Laura Kodytek, TU Dortmund, 2016
  "Optische Spektroskopie an Wolframdisulfid-Monolagen"

Acknowledgements

Finally, I would like to express my gratitude to all the people that supported me on my way towards this thesis and accompanied me along this exciting journey. I am particularly thankful to..

- ... My advisor Prof. Dr. Markus Betz for giving me the opportunity to work at E2b and providing guidance, motivation and advice way beyond this thesis at all times.
- ... Jan Lohrenz and Claudia Ruppert for avidly introducing me to experimentation in the lab and offering their knowledge and support in the early stages of my scientific career.
- ... The current and former members of E2b. Working together with you has been a most pleasant and an enriching experience. Special mentions belong to Elmar Sternemann, Thorben Jostmeier, Sergiu Anghel, Felix Passmann, Laura Krauß-Kodytek and Jan Mundry for their remarkable team spirit and many fondly remembered scientific and not so scientific discussions.
- ... Prof. Dr. Manfred Bayer and all colleagues from E2 for the positive working atmosphere at the department.
- ... Prof. Dr. Alan Bristow for being a great source of inspiration and motivation during his collaborative stay at our department.
- ... Michaela Wäscher for the administrative support and Dirk Schemionek for the kind assistance in sample preparation.
- ... My family, especially my parents Lothar and Evelin and my brother Matthias for their unwavering support and without whom this achievement wouldn't have been possible.
- ... Lana for her unconditional love and encouragement at all times during my years of studies and research.
- ... My friends from the "Schwafelrunde" who I feel very lucky to have acquainted over the years of my stay at TU Dortmund and am happy to have shared this journey with.